Enhanced Display of Mitoses in Hematoxylin-Eosin Digital Pathology Images

John Heerfordt Sjöqvist

A thesis presented for the degree of
Master of Science in Biomedical Engineering

LUND
UNIVERSITY

Department of Biomedical Engineering, Lund University
Sweden, 20th June 2016
Supervisor: Einar Heiberg

Sectra Imaging IT Solutions
SECTRA

Abstract

Identifying mitotic figures in digital pathology images is useful in diagnosis and prognosis of cancer. The task itself is time consuming and sometimes difficult for pathologists. Recent research has focused on machine learning for automatic detection of mitoses. The aim of this work was to apply image processing to facilitate ocular examination of mitotic figures in hematoxylin and eosin stained images, since such an approach can be adopted faster in clinical applications.

Several contrast adjustment algorithms were considered including contrast limited adaptive histogram equalization (CLAHE) and local Laplacian filters. The classic sharpening method unsharp masking was also used. Processing was done in the HSV and L*a*b* colour spaces and to channels of images where the stains hematoxylin and eosin had been separated through colour deconvolution. For validation a senior pathologist scored images with respect to the details of mitoses and general image quality.

In the scoring unsharp masking obtained the best results with significant improvements of both the details of mitotic figures and general image quality. Local Laplacian filters and CLAHE improved the general image quality but only slightly improved the details of mitotic figures. CLAHE occasionally resulted in unwanted darkening of both mitoses and the image as a whole. The same algorithm applied to the hematoxylin channel of images showed potential although it requires careful estimation of the colour matrices that are used to deconvolve histopathology images into stain components.

No investigated algorithm can alone eliminate the pathologists difficulties concerning mitotic figures. However, image enhancement may reduce the time needed for examination.

Keywords: Digital Pathology · Cancer · Mitosis · Mitotic Figure · Contrast Limited Adaptive Histogram Equalization · Unsharp Masking · Local Laplacian Filters · L*a*b* · HSV · Colour Deconvolution

Bildbehandling av mitoser

Populärvetenskaplig sammanfattning

I digitala bilder av vävnadsprov finns en klar relation mellan celldelningar och cancer. Att avgöra om vissa strukturer är cellkärnor i delningsfas eller inte, kan vara svårt. Detta arbete avsåg bildbehandling av skärpa och kontrast för att underlätta medicinsk bedömning.

Cancer är en av våra dödligaste sjukdomar. När cancer diagnostiseras tas vanligen biopsier som sedan analyseras av en patolog. Traditionellt har de undersökningarna gjorts i mikroskop, men på senare tid har digital patologi introducerats på sjukhus runt om i världen. Vävnadsprovet skannas med dedikerade skannrar varefter undersökning kan ske på en datorskärm. Fördelarna är många; såsom möjligheterna att lagra bilder i sökbara databaser och att använda digital bildbehandling. Bland nackdelarna kan nämnas att digitala bilder oftast har ett enda fokuslager för varje skannad förstoring. Dessutom saknas i många digitala visningsprogram en direkt motsvarighet till den belysningsknapp som finns på klassiska mikroskop.

En struktur som patologerna letar efter vid cancerdiagnostik är mitoser, cellkärnor som delar sig. Mitosernas utseende och antal kan nämligen kopplas till cancertyp och malignitet. Om många celler delar sig på liten yta, är det ett tecken på hög aktivitet i vävnaden, förknippat med elaka tumörer. Att undersöka och räkna mitoser tar tid och kan vara svårt. För att snabba på den processen undersökte detta arbete bildbehandlingsalgoritmer för att göra det lättare att identifiera mitoser.

För att förstå svårigheterna med undersökning av mitoser, intervjuades två patologer. Därefter applicerades kontrast- och kantförbättring på digitala patologibilder för att avhjälpa de problem som patologerna angivit. Arbetet avslutades med att en patolog jämförde behandlade bilder med obehandlade. Bilderna betygsattes utifrån generell bildkvalitet och detaljrikedom i mitoserna. Tre olika algoritmer utvärderades; två som ändrar kontrast och en som påverkar skärpa. Statistisk förbättring av mitosernas detaljer och den generella bildkvaliteten kunde visas när skärpan justerades. Vid kontraständringar kunde enbart förbättrad generell bildkvalité konstateras.

En kontrastjusteringsalgoritm, kontrastbegränsad histogramutjämning (CLAHE), har integrerats i företaget Sectra Imaging IT Solutions AB:s mjukvara för visning av digitala patologibilder. Företagets system baseras på en klient-server. CLAHE

körs på servern i samband med att den del av patologibilden som visas på skärmen, hämtas till klienten.

Enskilda cellager som fixerats på objektglas är näst intill transparenta. På grund av detta infärgas vävnadsproverna med färgämnen som har varierande affinitet för olika slags cellulära strukturer. I detta arbete har enbart vävnad som färgats med hematoxylin och eosin använts, vilket ger rosa-lila bilder. I intervjuerna framkom att patologerna önskade att färginnehållet inte skulle förändras. Därför användes framförallt representationer av digitala bilder där färginnehåll och intensitet separerats. På så vis är det möjligt att enbart bildbehandla bildernas intensitet.

Att mitoser och området runt dessa tenderar att vara mörkare än andra strukturer visade sig ha stor påverkan på lämplig bildbehandling. Många algoritmer gjorde mitoserna och deras omgivning ännu mörkare vilket gör det svårare att se detaljer. Förklaringen är algoritmernas strävan efter att maximera utnyttjandet av alla tillåtna intensitetsvärden.

Arbetets slutsats är att ingen av de utvärderade algoritmerna ensam kommer att eliminera patologernas problem med undersökningar av mitoser. Pågående teknisk utveckling av bilder med högre upplösning och flera fokuslager, i kombination med bildbehandling bedöms vara en mer trovärdig lösning.

Acknowledgements

Albert Einstein once said “Information is not knowledge. The only source of knowledge is experience.” People surrounding me have kindly shared their experiences throughout my work. Thanks to...

- my academic supervisor Dr Einar Heiberg (Lund University) for guidance and always having ideas.
- Tobias Dahlberg, my supervisor at Sectra Imaging IT AB, for the introduction to digital pathology, programming tips and support.
- the pathologists who contributed with clinical and medical expertise.
- all staff at Sectra, the company where this project was carried out.
- family and friends.

Nomenclature

Abbreviations

CLAHE	contrast limited adaptive histogram equalization
HSV	hue saturation value
RGB	red green blue
SSEQ	spatial-spectral entropy-based quality
WSI	whole-slide imaging

Mathematical Notation

$*$	convolution operator
$\lceil \cdot \rceil$	ceiling function
$\{\}$	set
$\{G_l[I]\}$	Gaussian pyramid of image I
$\{L_l[I]\}$	Laplacian pyramid of image I
$\mathbb{N}$	natural numbers
$\mathbf{X}$	matrix
$\mathbf{x}$	vector
`downsample`$(\cdot)$	low pass filter and downsample image by two operator
`upsample`$(\cdot)$	upsample image by two with smooth kernel operator
$\|\|\mathbf{X}\|\|$	Euclidean norm of matrix
$\|\|\mathbf{x}\|\|$	Euclidean norm of vector
`collapse`$(\cdot)$	Collapse Laplacian pyramid

Contents

Chapter 1

Introduction

The digitalization of society has reached the medical discipline of pathology. The word *pathology* is formed of two components from ancient Greek, *pathos* and *logia* [1, p.1]. Literally the meaning is the *study of suffering*. In this text it refers to the medical speciality where tissue and body fluids are examined to gain clinical information. Traditionally pathologists have examined tissue specimens with a light microscope to identify signs of disease [2, p.6]. There are many benefits of instead displaying tissue samples on a computer screen, such as systematic annotation, simpler storage, increased ergonomics and possibilities to use digital image analysis. However there are still shortcomings in the quality of the digital images.

Cancer is a global health problem. According to the World Health Organization's *World Cancer Report 2014* more than eight million people died from cancer-related complications 2012 [3]. Assessment of cancer is the most common task for pathologists. The increasing number of cancer cases put a huge strain on pathology departments worldwide. Hence any speed-up of diagnostication will save lives.

The overall aim of this thesis was to enhance the display of digital pathology images. For successful enhancement it was considered a good approach to focus on a particular worktask for pathologists. Counting and examining mitoses, cell nuclei that divide, is common during cancer diagnostics. Therefore, enhancing the display of mitoses was the final goal.

The project was carried out during spring 2016 at Sectra Imaging IT Solutions AB in Linköping, Sweden. Sectra provides IT solutions in the field of medical imaging. The large product portfolio comprises a complete digital pathology solution, including a picture archiving and communication system and a viewer software.

The thesis starts with an introduction to the field of digital pathology, colour spaces and selected image enhancement techniques in Chapter 2. Chapter 3 covers the objectives of the thesis. Identification of image-related clinical problems and an attempt to solve one of them (counting of mitoses) are presented in Chapter 4. The results are reported and discussed in Chapter 5 and 6 respectively. Finally future work in image processing of digital pathology images is covered in Chapter 7 before concluding remarks are made in Chapter 8.

Chapter 2

Background

Pathologists examine tissue and cells mounted on glass slides. There are two main fields of pathology, histopathology and cytopathology. In histopathology sliced tissue, thus keeping structural information, is examined whilst cells in solution are observed in cytopathology. Histopathology is the field concerned in this work.

2.1 Histopathology

After taking a biopsy from a patient, it cannot be mounted on a microscope slide straight away. First preprocessing is necessary including fixation of the tissue, replacing water with alcohol and impregnating the specimen in wax [4, p.8]. Without these steps the tissue would degrade over time and be extremely sensitive. From the specimen covered in wax, sections as thin as 3-12 μm are cut and subsequently mounted on the slides [4, p.9]. Tissue mounted on slides is shown in Figure 2.1(a).

2.1.1 Staining

A single cell layer mounted on a slide is so thin that it appears transparent. Hence using brightfield techniques, i.e. illuminating the tissue from below, the output would be blank. To obtain a coloured image one stains the tissue with dyes that colour tissue components. Since different structures have varying affinity for the stains, image formation is possible.

There are many different stains that can be applied to a tissue section. The most widely used stain is the hematoxylin-eosin stain which consists of the two dyes hematoxylin and eosin after another. Hematoxylin targets especially acidic structures and is purple-blue in colour. Eosin on the other hand targets proteins in general and basic proteins in particular. It provides a pink-red colouring [4, p. 10]. Viewing a specimen stained in this way nuclei turn out blue or purple, cartilage and basophilic cytoplasm purple, cytoplasm and collagen pink and red blood cells and eosinophil granules bright red [4, p. 12].

(a) Tissue mounted on glass slides [5]

(b) Light microscope [6]

Figure 2.1: Histopathology essentials

2.1.2 Magnification

The nuclei of human cells are small, typically 7-12 μm [4, p.3]. This implies that magnification is necessary to see them. In a light microscope (cf. Figure 2.1(b)) magnification occurs both in the objective lens and the eyepiece. The magnification of the objective lens is usually specified as 10X, 20X, 40X and so forth. On top ten times additional magnification occur in the ocular. Observing a specimen with the 40X setting for the objective lens thus gives 400 times magnification.

2.1.3 Digital Pathology

What is digital pathology? According to the United States Digital Pathology Association "Digital pathology is a dynamic, image-based environment that enables the acquisition, management and interpretation of pathology information generated from a digitized glass slide" [7]. Regarding the clinical applications, the same organisation suggests that "Healthcare applications include primary diagnosis, diagnostic consultation, intraoperative diagnosis, medical student and resident training, manual and semi-quantitative review of immunohistochemistry, clinical research, diagnostic decision support, peer review, and tumour boards" [7].

There are various types of digital pathology of which the simplest probably is conversion of a light microscopy image into a digital format. In this text, *digital pathology* refers to digital images obtained by scanning slides with dedicated scanners. That process is called whole-slide imaging (WSI) [8, p. 6]. A slide scanner is shown in Figure 2.2. The digitized slides can thereafter be viewed at a computer workstation (cf. Figure 2.3) [9].

Standard slides are 1 x 3 inches although some scanners can process larger ones as well [8, p. 18]. The magnification levels in light microscopy has been mimicked in digital pathology. In digital pathology the display pixel spacing affects the perceived magnification but basically 40X digitally and classically shall be the same.

Figure 2.2: Hamamatsu Nanozoomer scanner (Courtesy of Hamamatsu Photonics K.K)

In whole-slide imaging a large number of small images are stitched together to form an image of the whole slide. This is done since digital pathology images are incredibly large. Before compression a standard image may require about 40 GB of storage, although it can be reduced to 2-3 GB with lossy compression. Image widths and heights of 100 000 pixels in each direction are typical. There are different approaches to stitching images, tile and line scanning. In the former a number of rectangular tiles are scanned and in the latter strips are combined to form the whole-slide image [8, p. 18]. Different tiles within the same slide may end up with different quality.

Figure 2.3: Pathologist examining a tissue section at a computer workstation. (Courtesy of Sectra Imaging IT Solutions AB)

To enhance the display performance it is common to use a pyramidal storage format. Several zooms of the originally scanned image are stored, enabling quick rendering of an image by using the zoom that is closest to the current display zoom level [8, p. 20]. As an example, assume that the the viewer software displays a tissue section in low magnification such as 10X. If precomputed low-resolution images would not be available, it would be necessary to merge a large number of tiles from the highest resolution and downsample the result. This is avoided by storing the same image in

multiple resolutions. The main disadvantage of the pyramidal format is the increased file size.

2.2 Cell Division and Cancer

Many examinations at pathology departments are done to determine if a tumour is present in a tissue sample and if so what particular type. Tumours are tightly connected to cell division which is covered in the paragraph below.

2.2.1 Cell Division

Human cells are eukaryotic cells which by definition have nuclei. The nucleus consists of concentric membranes and contains the DNA [10, p. 17]. The DNA molecules are folded around proteins for compression, forming a complex called chromatin [11, 179]. Condensed chromatin forms the chromosomes. The cell cycle is the process of duplication and division that allows organisms to grow. In the cell cycle the nucleus divides into two during mitosis and the cell divides into two during cytokinesis. An overview of cell division, from the replication of DNA until mitosis and finally cytokinesis, is seen in Figure 2.4.

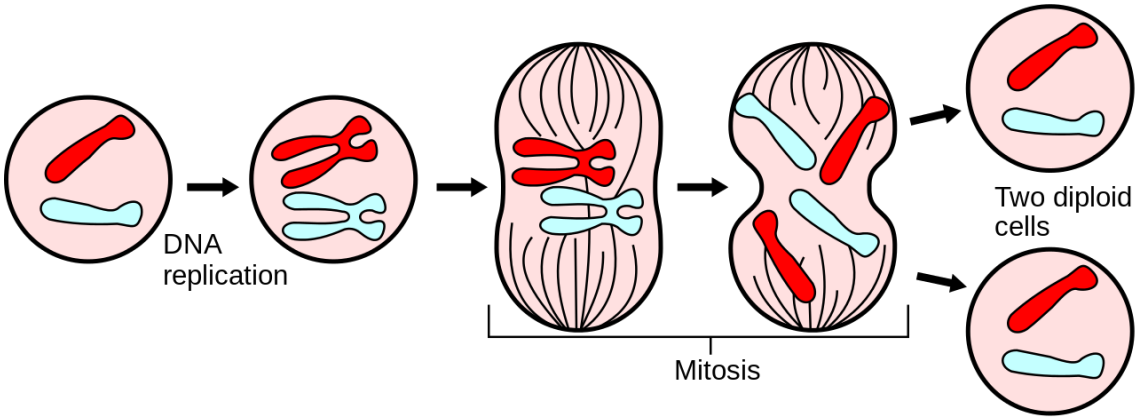

Figure 2.4: Cell division including mitosis. The result after cytokinesis is two genetically identical cells.

Mitosis is divided into five phases. A good description is found in [11, pp.622-623]. These phases are (cf. Figure 2.5):

- Prophase: The duplicated chromosomes condense.
- Prometaphase: The nuclear envelope is broken down and a structure called the mitotic spindle attaches to the chromosomes in order to move them.
- Metaphase: All chromosomes have been aligned by the mitotic spindle.

- Anaphase: Sister chromatids, i.e. two identical copies of a chromosome after replication, separate.
- Telophase: The two sets of chromosomes are encapsulated by one nuclear envelope each resulting in two genetically identical nuclei.

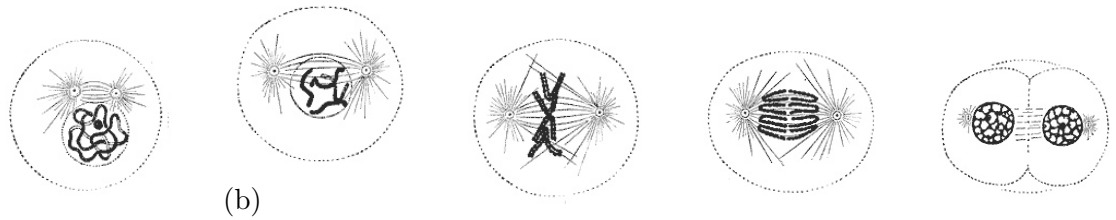

(a) Prophase (b) Prometaphase (c) Metaphase (d) Anaphase (e) Telophase

Figure 2.5: Different stages of mitosis.

2.2.2 Cancer

Cancer is a collection name for disorders related to abnormal cell growth and division. Neoplastic cells are cells that replicate asynchronous to normal cells. A collection of neoplastic cells, i.e. a neoplasm, is usually called a tumour. The difference between a general tumour and cancer is that the latter is malignant. Malignant tumours tend to spread to adjacent tissue but may also metastasise to distant locations [1, p. 165]. The opposite of a malignant tumour is a benign where the likelihood of re-localization is low. In *Robbins Basic Pathology* several of the common characteristics of cancers are described [1]. Mutations of the DNA, having occurred spontaneously or as a result of environmental impact, is claimed to have a major role. These DNA alterations survive cell division allowing tumours to grow.

When cancers are diagnosed mitoses provide valuable information to pathologists. The occurrence, shape and number of mitoses are of concern. Many mitoses links directly to high proliferation rate [12]. The latter is a characteristic of malignant neoplasms. Besides mitoses, variability in cell size and shape, i.e. pleomorphism [1, p. 165], and the chromatin pattern is of interest. The chromatin in nuclei may look different in malignant cells [13].

2.2.3 Mitotic Figures

In hematoxylin-eosin images mitoses are often identified as dark shapes due to the condensed chromosomes. These are called mitotic figures. In Figure 2.6 the cell in mitosis is easily identified. To identify a mitosis there are several criteria. Some examples are absence of nuclear membrane, no clear zone in the center of the nucleus, hairy projections of the nucleus and basophilia of surrounding cytoplasm [12]. Basophilia is high affinity for basic dyes such as hematoxylin. The appearance of a mitosis depends on the stage of the process and the direction in which the tissue was sliced. Clinical applications of mitotic figures include:

- In soft tissue tumours mitotic count and necrosis are important predictors [1, p. 792]. In stomach tissue more than five mitotic figures per ten high power fields indicate malignancy of a tumour [14, p.297]. A high power field is an area unit. It is the observed area in a light microscope at four hundred times magnification, i.e. 40X [14, p.297].
- Histological grading are used in tumour assessment to tailor treatment plans and describe malignancy. The Nottingham Grading System, designed for breast cancer, considers tubule formation, nuclear pleomorphism and mitotic counts as relevant prognostic factors [15]. Normally the number of mitotic figures per ten high power fields are counted. [16].
- For cutaneuous malignant melanoma, i.e. a deadly type of skin cancer, mitotic rates reflect the outcome of patients [17].
- Anaplastic malignant tumours can be indicated by mitotic activity. Mitoses may be abnormal. As an example tripolar and quadripolar mitotic figures may show up [1, p. 165]. A tripolar mitotic figure is seen in Figure A.1(d).
- Dysplasia is abnormal proliferation that is non neoplastic. Dysplastic cells look a bit different from one another and mitotic figures are more common than in normal tissue [1, p. 166].
- In midgut carcinoid tumours presence of mitoses in combination with increased cell size and local invasion indicate is a bad sign [1, p. 578].
- The mitotic activity is often high in neuroblastomas [1, p. 259], a type of cancer developing in nerve tissue.

Unfortunately there are other structures that look similar to mitoses, making it hard to be certain whether some dark shapes are mitoses or not. As an example apoptotic cells, i.e. cells undergoing a form of programmed cell death, can be taken for mitotic figures. In slides of low image quality, pycnotic, hyperchromatic and deformed nuclei [12] can appear like mitotic figures. A pycnotic nucleus has shrinked in size and its chromatin has thickened. A hyperchromatic nucleus is abnormally highly coloured and may indicate anaplasia, which is lack of cell differentiation.

In the consensus statement *Prognostic factors in breast cancer* from the College of American Pathologists, a number of recommendations regarding mitotic index were presented [18]. First of all the number of mitotic figures should be counted in the part of the tumour with the highest activity in ten consecutive high power fields. Moreover only definite mitotic figures should be counted. This text was published before the era of digital pathology. Therefore, how to measure the size of high power fields were covered. This is not a concern in the digital environment because areas can be measured easily.

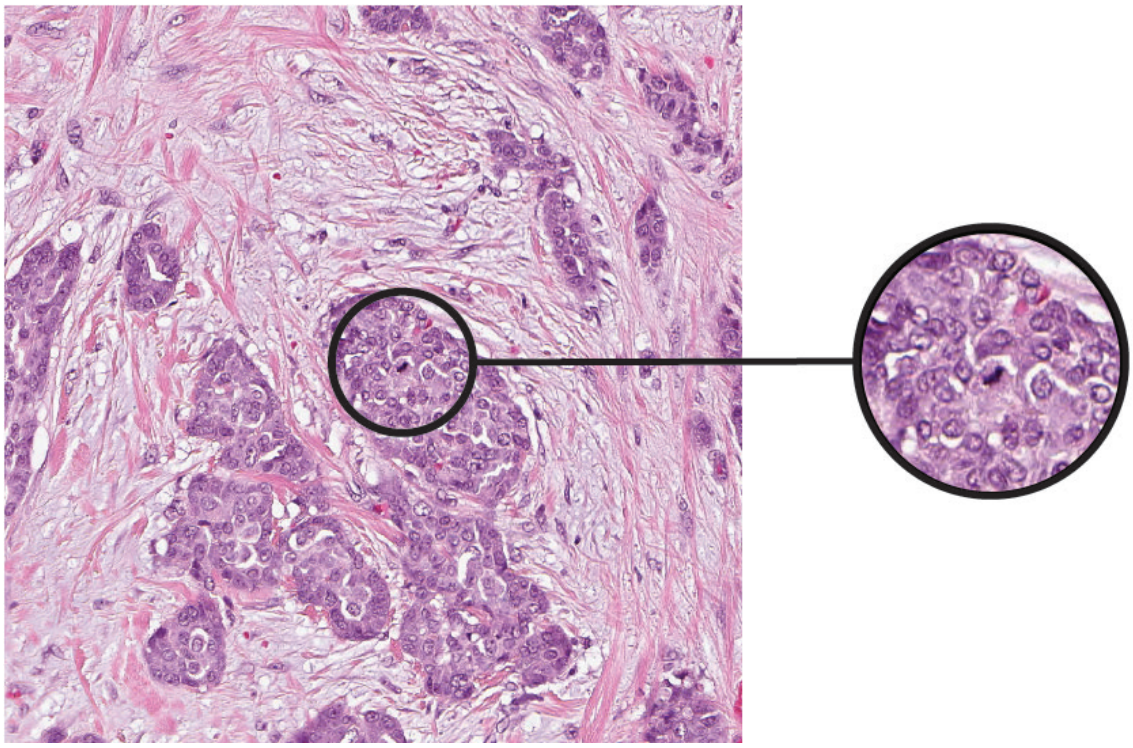

Figure 2.6: A mitotic figure in breast tissue scanned at 20X. The mitotic cell is the dark shape in the centre of the black circle. The normal use of 40X images for examination of mitoses is understandable.

2.3 Colour Spaces

Digital processing of grayscale images is straightforward whilst colour images require more consideration. Separate processing of each colour channel may result in a very different output in terms of perceived colour. Before a brief explanation of some useful colour spaces, two key image features should be clarified. An image's contrast depends on the difference between the highest and lowest intensities in combination with how effectively the values within that range are used. Large maximal difference and even distribution of pixel values mean good contrast. The number of unique pixel values in an image forms the dynamic range [19, p. 40].

Three popular colour spaces that have been used in this work are summarized below. Later a colour representation that is specific to stained images will be presented (cf. Section 2.4.4).

2.3.1 RGB

A widely used colour space is RGB where colours are described as a sum of red (R), green (G) and blue (B). RGB is an additive model where R = 0, G = 0 and B = 0 corresponds to the darkest black, to which the primary colours can be added. The values are nonnegative and have a maximal possible value [19, p. 240-241]. The

most common is 24 bit colour images yielding 8 bits per channel. Hence the normal range is 0-255.

2.3.2 HSV

There are several colour spaces that separate a pixel's intensity from its colour. These are more intuitive than the RGB representation for image processing purposes. The HSV colour space is one such example with the components hue (H), saturation (S) and value (V). It is also referred to as HSB, where B is for brightness [19, p. 258]. Brightness/value is the intensity of a colour, hue describes the perceived colour by an observer and saturation is a measure of relative purity. The term chromaticity includes both hue and saturation [20, p. 286]. Normally the hue is given in degrees $0° - 360°$ and saturation and value are in the range 0-1.

2.3.3 L*a*b*

The L*a*b* colour space is similar to HSV in separating the intensity from the chromaticity. L^* represents the intensity or lightness, a^* red-green colours and b^* green-blue colours [20, p. 322-323]. The L*a*b* colour space was originally designed to vary linearly with human colour perception [19, p. 281]. Usual ranges are $L^* \in [0, 100]$ and $a^*, b^* \in [-100, 100]$. There are several alternative versions of the colour space. Here L*a*b* refers to the CIE 1976 version.

In Figure 2.7(a)-(c) a hematoxylin-eosin image and plots of the corresponding datapoints in the HSV and L*a*b* colour spaces are depicted. Note that a very limited part of the colour spaces are used due to the staining.

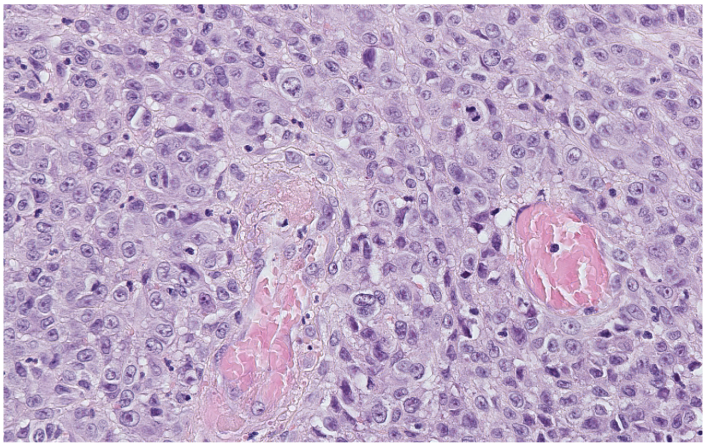

(a) A hematoxylin-eosin image

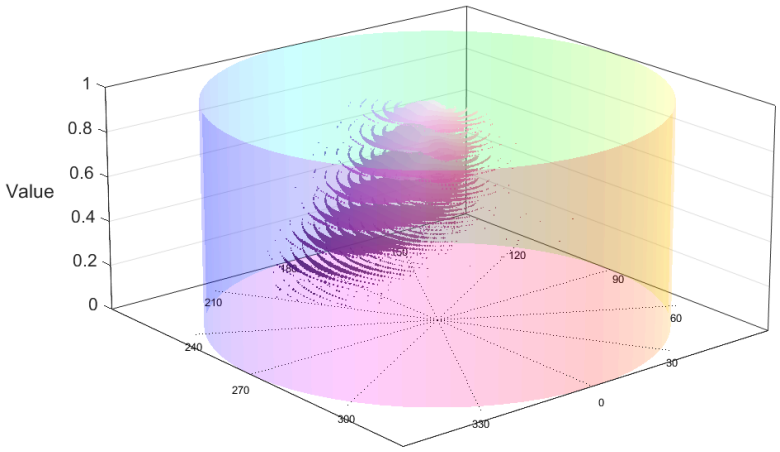

(b) HSV datapoints

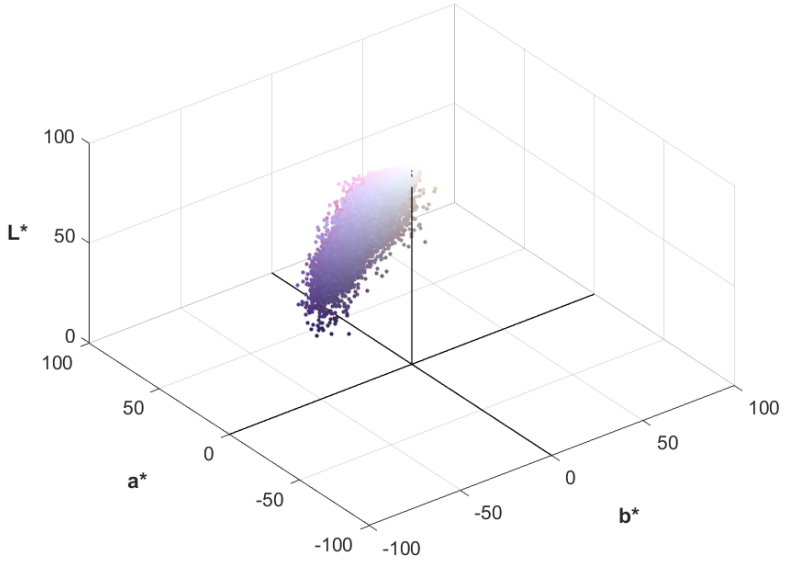

(c) L*a*b* datapoints

Figure 2.7: A hematoxylin-eosin image (a) and plots of the pixels in the HSV (b) and L*a*b* (c) colour spaces.

2.4 Image Enhancement

A digital colour image can be seen as a two-dimensional array of pixels, each with a specific chromaticity and intensity. Histograms can be used to represent the localization of the intensity and chromaticity values. A histogram is basically an array where each entry corresponds to a specific value or a range of values. The value of an entry is the number of occurrences of the value(s) that the entry corresponds to in the image (cf. Figure 2.8). The notation for histograms are adopted from the books on digital image processing by Burger and Burge [19, pp.37-62] and Gonzalez and Woods [20, pp. 88-94]. The histogram of the image I will be denoted h.

A mathematical formulation of a histogram in the case where the pixel values are natural numbers is

$$h(i) = |\{(x, y);\ I(x, y) = i\}|, \quad i \in \mathbb{N} \tag{2.1}$$

where the cardinality operator $|\cdot|$ gives the number of elements in the set and x and y are the pixel coordinates. If the pixels take continuous values, each bin of the histogram will instead refer to an interval of values.

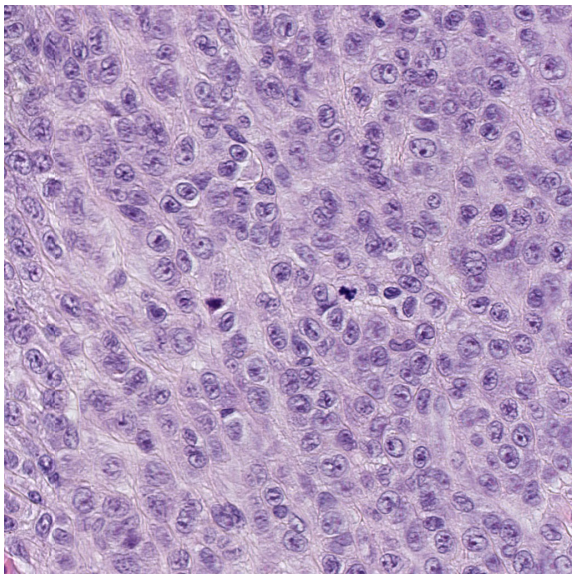

(a) Mitotic figures in image with 1024 x 1024 pixels scanned at 40X.

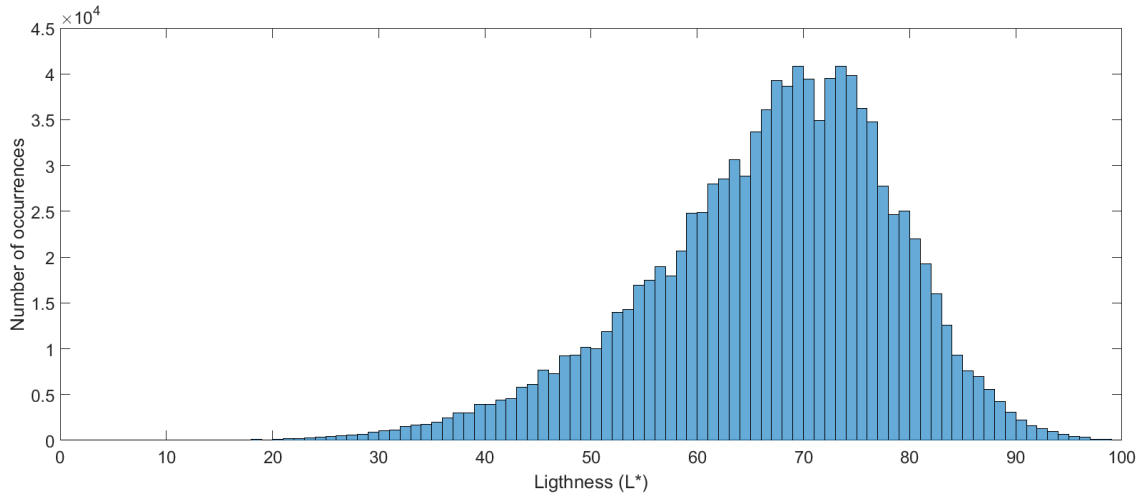

(b) Histogram of the L* channel

Figure 2.8: An image with two candidate mitotic figures (a) and the corresponding histogram of the L* channel in the L*a*b* colour space (b).

Sometimes histograms are normalized by dividing the histogram entries by the total

number of pixels in the image I. The normalized histogram $\tilde{h}$ is thus obtained as

$$\tilde{h}(i) = \frac{h(i)}{N} \tag{2.2}$$

where N is the total number of pixels in the image. In this case the histogram can be seen as the discrete probability density function of the pixel values.

2.4.1 Histogram Equalization

Histogram equalization is the foundation for several contrast enhancement algorithms relying on histograms. It is here first introduced in the continuous domain for simplicity, and thereafter discretized. The description below is from Gonzalez and Woods [20, p. 91-94]. Let $I(x, y) = r$ be the intensity of a pixel normalized to the interval $[0, 1]$. Histogram equalization can be seen as a point operator $T(\cdot)$ working on the intensity values. The output intensity after applying the operator will be called s.

$$s = T(r), \quad 0 \leq r \leq 1 \tag{2.3}$$

It is necessary that the output of $T(\cdot)$ is confined to the interval $[0, 1]$ for input in the same range and that each argument $r \in [0, 1]$ is mapped to at most one value. It is convenient to think of r and s as random variables with corresponding intensity probability density functions p_r and p_s respectively. If the conditions on $T(\cdot)$ holds the densities can be related as,

$$p_s(s) = p_r(r)|\frac{dr}{ds}| \tag{2.4}$$

One possible transformation is simply the cumulative distribution function of the intensities in the image.

$$s = T(r) = \int_0^r p_r(w)dw \tag{2.5}$$

It can be showed by inserting the mapping (2.5) into (2.4) and applying Leibniz's rule that this transformation turns s into a uniform random variable on the interval $[0, 1]$, i.e. $p_s(s) = 1, \quad 0 \leq s \leq 1$.

In digital image processing the discrete counterpart of this transformation is of practical interest. It is described by

$$s_k = T(r_k) = \sum_{j=0}^{k} p_r(r_j) = \sum_{j=0}^{k} \frac{n_j}{n}, \quad k = 0, 1, 2, ..., L - 1. \tag{2.6}$$

for an image with L possible intensity levels where r_k is the intensity of a specific input pixel, s_k the corresponding output and n the total number of pixels. It is worth emphasizing that in general the result of the discrete method will not be a perfect discrete uniform random variable. In Figure 2.9 an example of a mapping function obtained as the cumulative sum of a histogram can is depicted. The mapping has been multiplied with a factor one hundred to allow application to L^* intensities yielding $T: \ r \in [0, 100] \rightarrow s \in [0, 100]$.

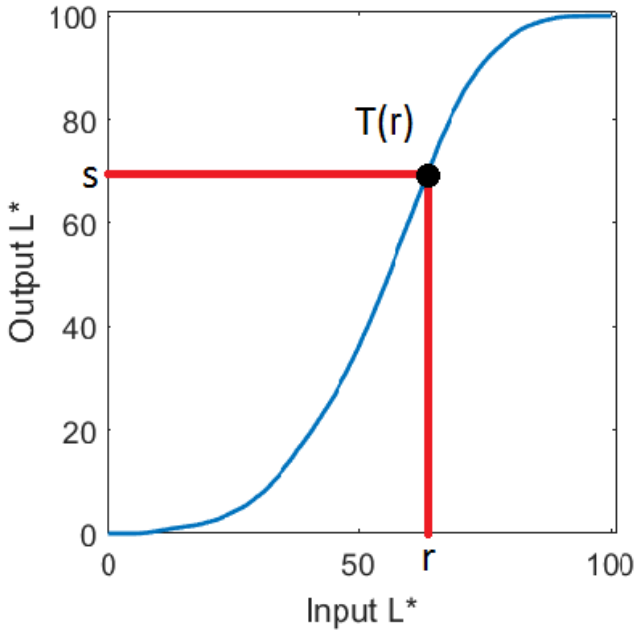

Figure 2.9: Mapping function for histogram equalization of L* channel.

Histogram equalization increases the global contrast of images. However it is sometimes inadequate. Consider for example a gray-scale image with a small dark object on bright background. Here histogram equalization would force the pixels in the background that were a bit more dark gray than the others to become black to achieve a uniform histogram.

2.4.2 Adaptive Histogram Equalization

Adaptive Histogram Equalization is a more sophisticated version of histogram equalization, adjusting local instead of global contrast. The image is divided into tiles for which the cumulative distribution functions are calculated. Pizer *et al.* suggested to calculate the mappings on a rectangular grid of pixels [21]. Thereafter bilinear interpolation is used to find the new output values. For a pixel at position (x, y) taking the value r, the suggested mapping is

$$s = a\Big(bT_{ul}(r) + (1-b)T_{ur}(r)\Big) + (1-a)\Big(bT_{ll}(r) + (1-b)T_{lr}(r)\Big) \tag{2.7}$$

where T_{ul}, T_{ur}, T_{ll} and T_{lr} are the mappings for the upper left, upper right, lower left and lower right contextual regions respectively. a and b are distance-related scale factors

$$a = \frac{y - y_-}{y_+ - y_-}$$

$$b = \frac{x - x_-}{x_+ - x_-}.$$

Here x_-, x_+, y_- and y_+ refer to the x and y coordinates of the centres of the neighbouring tiles as illustrated in Figure 2.10. At the image boundaries special cases occur. It is necessary to distinguish between corner, border and inner parts of the full image.

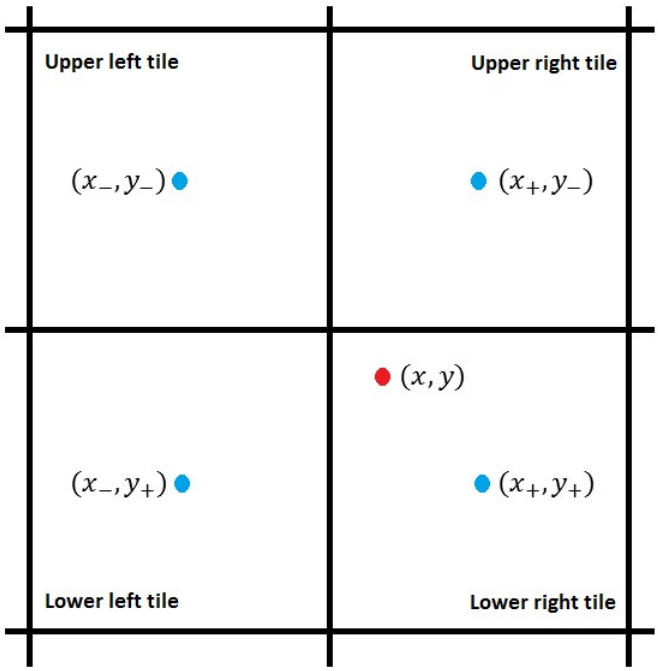

Figure 2.10: Drawing illustrating the position of the tile centres (blue) in relation to a pixel at position (x, y) (red). Standard image processing coordinates with the origin in the upper left corner is assumed.

2.4.3 Contrast Limited Adaptive Histogram Equalization

Adaptive histogram equalization has a problem with amplification of noise. Contrast Limited Adaptive Histogram Equalization (CLAHE) uses a modification to solve that problem. Adaptive histogram equalization mainly introduces noise in homogeneous areas, where many pixels have intensity values in the same range. The contrast limitation in CLAHE consists of clipping the local histograms at a fixed

level. The excess pixels are thereafter uniformly redistributed over the full range of possible intensity values [22]. The concept is illustrated in Figure 2.11.

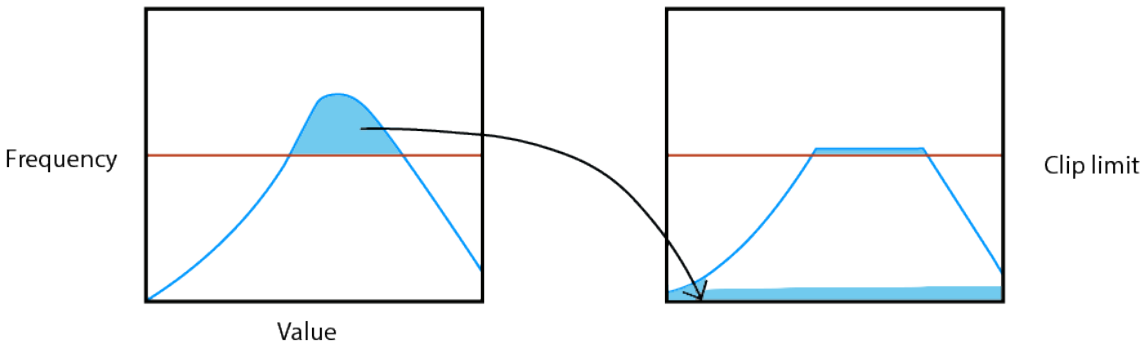

Figure 2.11: The result of clipping a histogram and uniform redistribution of the pixel values. Some pixels are exceeding the clip limit after the redistribution.

CLAHE uses two main parameters. Exactly as in adaptive histogram equalization one has to select the number of tiles. Moreover the clip limit has to be set. In many image processing libraries, e.g. MATLAB [23], a normalized clip limit in the range $[0, 1]$ is entered. From that input the actual clip limit used in the algorithm is computed as

$$c = c_{min} + \text{round}(c_{normalized} \cdot (N - c_{min})). \tag{2.8}$$

Here round$(\cdot)$ rounds to the nearest integer, N is the number of pixels in a tile given as the product of rows and columns and c_{min} is the minimal possible clip limit, i.e. $\lceil \frac{N}{\text{numBins}} \rceil$. *numBins* is the number of bins in the histogram used to construct the mapping. Since the clipping procedure takes place before the mappings are computed, the minimal clip limit corresponds to calculating the mapping from a uniformly distributed histogram. That is the opposite of no clipping where the goal is to achieve a uniform histogram. If the normalized clip limit $c_{normalized}$ is set to one, the clip limit equals the number of pixels in the tile meaning no clipping. With a low value for the normalized clip limit the contrast enhancement is limited whilst with a very high value CLAHE simplifies to adaptive histogram equalization. Algorithm 1 gives the pseudo-code of the process.

Figure 2.11 also illustrates another issue. If all pixels above the clip limit are distributed equally over the whole dynamic range it will result in a histogram where there are still bins exceeding the limit. That is not a problem as it can be solved by iterating the process.

Algorithm 1 Contrast limited adaptive histogram equalization.

input: Original image, number of tiles, normalized clip limit
output: Contrast enhanced image
Divide image into tiles.
Compute clip limit.
for all tiles **do**
  Calculate histogram.
  Clip histogram according to clip limit.
  Compute mapping for the tile.
end for
for all pixels in image **do**
  Map pixel intensity value using mappings of neighbouring tiles.
  Interpolate between mapped intensity values.
end for

2.4.4 Colour Deconvolution

A histopathological image in RGB format can be converted to a colour space where the stains are separated. The method was originally suggested by Ruifrok and Johnston [24] which is the source of the following description. Two assumptions are necessary:

- Images obtained with RGB camera with *gamma* around one. Gamma refers to the exponent in the power-law describing the image capturing process [20, p. 81].
- Intensities on the R, G and B channels depend linearly on the fraction of transmitted light.

Light interaction in matter, e.g. a histologic specimen, can be described by Beer-Lambert's law

$$\mathbf{r} = \begin{bmatrix} I_R \\ I_G \\ I_B \end{bmatrix} = \begin{bmatrix} I_{0,R} e^{-A\mu_R} \\ I_{0,G} e^{-A\mu_G} \\ I_{0,B} e^{-A\mu_B} \end{bmatrix} \tag{2.9}$$

where I_c and $I_{0,c}$ are the light intensities leaving and entering the specimen respectively, measured on RGB channel c. μ_c is the absorption factor of a stain in channel c and A the amount of the stain. Hence there is a non-linear relation between the amount of stain and the measured values on the RGB channels. Assuming that hematoxylin and eosin were used for staining, both stains will contribute with a different amount to each of the RGB channels. Normally one incorporate a third channel in the model for light interaction with unstained tissue and to compensate for model errors. An orthogonal residual "stain" vector can be obtained as the cross-product between the hematoxylin and eosin vectors. The cross-product can result in negative entries which is unrealistic from a physical viewpoint. "Stains cannot

absorb a negative amount of light and there cannot be a negative amount of stain", as Macenko *et al* expressed it [25]. A compact summary of the original method was outlined in that same article on normalization of histology slides [25]. RGB values are converted to optical density as

$$\mathbf{v}_{OD} = -\log_{10}(\mathbf{r}) \tag{2.10}$$

where $\mathbf{r}$ is a 3 x 1 vector containing the RGB values scaled to [0, 1]. The optical density vector $\mathbf{v}_{OD}$ is assumed to be generated as a matrix multplication of the 3 x 3 stain matrix $\mathbf{V}$ and the 3 x 1 vector with stain saturations $\mathbf{v}_s$.

$$\mathbf{v}_{OD} = \mathbf{V}\mathbf{v}_s \Rightarrow \mathbf{v}_s = \mathbf{V}^{-1}\mathbf{v}_{OD} = \mathbf{D}\mathbf{v}_{OD}. \tag{2.11}$$

Here the columns of the stain matrix $\mathbf{V}$ contains optical density vectors for each stain and its inverse is the deconvolution matrix $\mathbf{D}$. There are several ways of obtaining the numerical values for the matrix entries in the colour matrix $\mathbf{V}$. The most exact is scanner specific and consists of scanning a slide with a single stain.

In Figure 2.12 the outcome is illustrated. The original image in (a) is deconvolved into three channels; hematoxylin, eosin and residual. These channels are seen in (b)-(d) where the single colour images are generated from each channel's intensity image. For interpretation purposes the hematoxylin grayscale image is represented in purple and the eosin counterpart in pink. The residual is displayed in bright green.

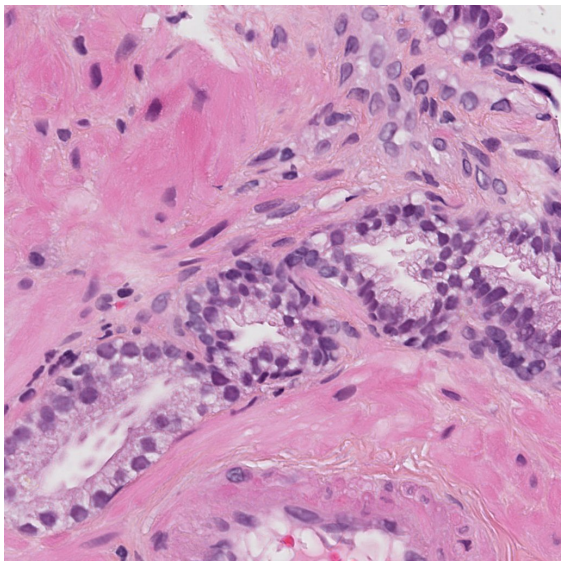

(a) Original image

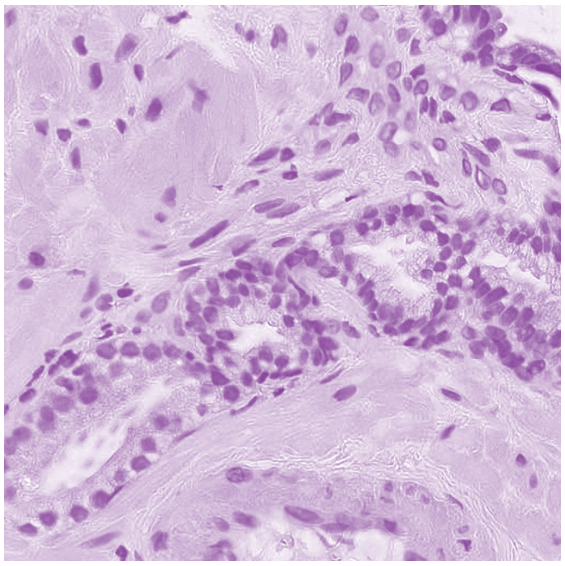

(b) Hematoxylin channel (purple)

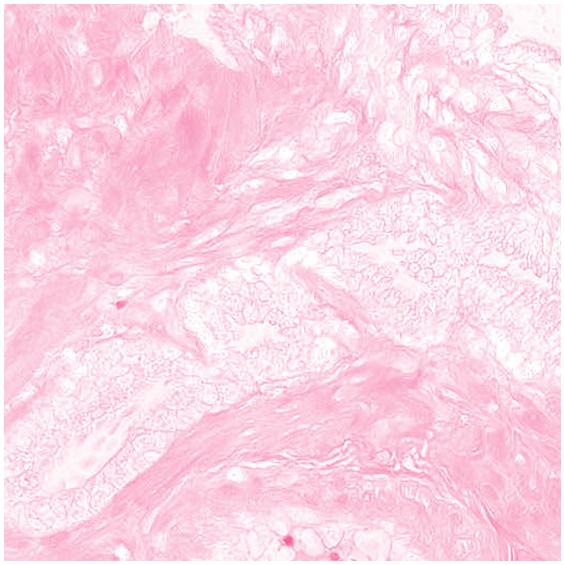

(c) Eosin channel (pink)

(d) Residual channel (green)

Figure 2.12: Example of colour deconvolution. The almost white residual image (d) indicates that the stain matrix is well matched to the image (a).

2.4.5 Image Sharpening

Before the era of digital imaging, processing of images was a real artwork. Photographs could be sharpened by combining a lowpass filtered (manually blurred) negative with the corresponding positive. The result of developing the clamped negative and positive was a sharper image.

The above mentioned procedure, called *unsharp masking*, can be mimicked digitally. To create an image where the edges are sharpened, a blurred version is subtracted from the original image. Smooth regions are less affected by the smoothing kernel than regions with edges and details, where pixel values change more quickly. This sharp image, called the mask, is added to the original image to increase its sharpness. In frequency domain this corresponds to constructing an image with a boost of the high frequency content and adding it to the original image. The description is adopted from [19, pp. 133-137]. Pseudo-code for unsharp masking is given in Algoritm 2. The filter h should blur the image. Gaussian filters are the most common [19, p. 134]. The scalar k adjusts the amount of sharpening.

Algorithm 2 Unsharp masking.

input: Original image $I_{original}$, smoothing filter h, scalar k
output: Sharpened image I_{sharp}
Generate mask: $M := I_{\text{original}} - (I_{\text{original}} * h) = I_{\text{original}} - I_{\text{blurred}}$
Add mask to sharpen the original: $I_{\text{sharp}} = I_{\text{original}} + k \cdot M$

2.4.6 K-means Clustering

If only pixels with certain characteristics are to be processed it is of interest to first cluster the image. K-means is probably the most classical clustering algorithm. A comprehensive description is found in *Pattern Recognition and Machine Learning* by Bishop [26, pp. 424-430], but the key concepts are introduced below.

In our context, the objective is to divide an images' pixels into K clusters (cf. the algorithm's name). Every single pixel $\mathbf{x}_i$ is considered to be a datapoint. Each cluster will have a center denoted $\mu_i,\ i = 1..K$. To cluster, the objective function J is minimized. It describes the distance between datapoints and their cluster's centroid. If K is the number of clusters and N the number of pixels, the objective function is

$$J = \sum_{n=1}^{N}\sum_{k=1}^{K} r_{nk}||\mathbf{x}_n - \mu_k||^2. \tag{2.12}$$

r_{nk} is an indicator-variable taking the value one when the centroid closest to datapoint $\mathbf{x}_n$ is μ_k and zero otherwise. The clustering is an iterative procedure. The centroids are normally initialized randomly whereafter the datapoints are assigned to the closest centroid. Subsequently the centroid is recomputed as the average of all the datapoints that it is responsible of. This procedure is repeated until convergence is reached. The method deals with vectors and hence RGB, L*a*b* or HSV values can be used as clustering input.

2.4.7 Image Pyramids and Local Laplacian Filters

As mentioned in Section 2.1.3, digital pathology images are usually stored in pyramidal format. Therefore it is of interest to investigate if image processing can benefit from this representation. Paris *et al.* suggested a contrast adjustment method using multiple resolutions of the same image in [27]. A summary of the technique, which relies on Gaussian and Laplacian pyramids, follows.

A Gaussian image pyramid consists of multiple versions of the same image but with different resolution and size. Conceptually, piling these images gives a pyramid. Let I denote the full resolution image and the set of images $\{G_l[I]\}$ its Gaussian pyramid. The bottom level is the full resolution image, i.e. $G_0 = I$, and the layers on top are of decreasing resolution and size. These low pass versions are created as $G_{l+1} = \texttt{downsample}(G_l)$ where the operator $\texttt{downsample}(\cdot)$ includes convolution with a smoothing Gaussian kernel and downsampling by a factor two. The pyramid concept is illustrated in Figure 2.13.

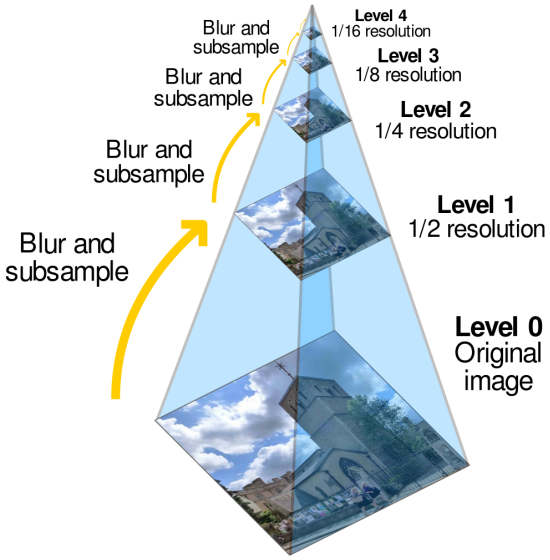

Figure 2.13: Illustration of Gaussian pyramid with five levels [28].

The Laplacian pyramid of the image I is denoted $\{L_l[I]\}$. Here the levels $\{L_l\}$ represent scale-varying details obtained as the difference between adjacent levels in the Gaussian pyramid, i.e. $L_l = G_l - \texttt{upsample}(G_{l+1})$. The operator $\texttt{upsample}(\cdot)$ does upsampling by a factor two with a smooth interpolation kernel. The highest level of the Laplacian pyramid is identical to the corresponding level of the Gaussian pyramid. In pyramid image processing the levels $\{L_l\}$ are processed separately, resulting in scale-varying effects. Finally, the enhanced version of the original image is obtained through a recursive procedure where the details in layer L_l are added to an upsampled version of the low pass layer G_{l+1}. This is called collapsing a pyramid. Mathematically the following is done for each layer: $G_l = L_l + \texttt{upsample}(G_{l+1})$. The operators $\texttt{downsample}(\cdot)$ and $\texttt{upsample}(\cdot)$ both use smooth kernels of size 5 x 5 pixels as suggested in the original article on Laplacian pyramids [29].

In the article by Paris and colleagues they introduced *Local Laplacian Filtering* as an edge-aware image processing algorithm. Edges in images are typically large discontinuities in the pixel values in a neighbourhood. The suggested method is able to enhance the details of the image without making edges neither smoother nor sharper. This is achieved with a user provided parameter σ, distinguishing edges from smaller details. First one computes the Gaussian pyramid of the input image. Then for each pyramid coefficient, i.e. a pixel in a pyramid, a point-wise remapping function is constructed and applied to the input image. Thereafter an intermediate Laplacian pyramid of the remapped image is computed. From the pyramid a single coefficient's value is extracted at the position corresponding to the location of the coefficient in the Gaussian pyramid. This value is stored in another Laplacian pyramid corresponding to the output image. In this way one coefficient in the output Laplacian pyramid is computed in each iteration. Algorithm 3 outlines the principle. The algorithm applies to both colour and grayscale images. In this work the colour version was used.

Algorithm 3 Local Laplacian Filtering

input: Original image I, σ
output: Image I'
Compute $\{G[I]\}$
for all coefficients (x, y, l), i.e. pixel at (x, y) in level l **do**
  $g \leftarrow G_l(x, y)$
  Create output buffer image $\tilde{I}$.
  for all pixels (u,v) of I **do**
    Apply remapping function: $\tilde{I}(u, v) \leftarrow r(I(u, v), g, \sigma)$
  end for
  Compute $\{L[\tilde{I}]\}$
  Update output pyramid: $L_l[I'](x, y) \leftarrow L - l[\tilde{R}](x, y)$
end for
Collapse output pyramid: $I' \leftarrow \texttt{collapse}(\{L_l[I']\})$

A key part of the method is the distinction that is made between fine-scale details and edges. The point-wise remapping function $r(\cdot)$ for colour images is

$$r(\mathbf{i}) = \begin{cases} r_d(\mathbf{i}, \mathbf{g}, \sigma) = \mathbf{g} + ||\mathbf{i} - \mathbf{g}||(f_e(||\mathbf{i} - \mathbf{g}|| - \sigma) + \sigma), & ||\mathbf{i} - \mathbf{g}|| \leq \sigma \\ r_e(\mathbf{i}, \mathbf{g}, \sigma) = \mathbf{g} + \frac{\mathbf{i}-\mathbf{g}}{||\mathbf{i}-\mathbf{g}||}\sigma f_d(\frac{||\mathbf{i}-\mathbf{g}||}{\sigma}), & \text{otherwise} \end{cases} \tag{2.13}$$

Details are thus distinguished from edges using a sphere of radius σ. The sphere is centred at $\mathbf{g}$ and then all colours outside is considered to be edges and all colours inside details. The function r_d is applied to details and r_e is used to remap edges. The two functions f_e and f_d are application dependent, but for detail enhancement it was suggested to use $f_d(\Delta) = \Delta^\alpha$ and $f_e(a) = a$. To compress or amplify edges it is possible to instead use $f_e(a) = \beta a,\ \beta \geq 0$ where $\beta > 1$ amplifies edges and $\beta < 1$ compresses edges. In case $\mathbf{i} = \mathbf{g}$ the second term in the bottom equation in (2.13) are set to the zero vector to avoid division by zero.

Local Laplacian filters are very computationally demanding but luckily the complexity can be reduced. Since only a small part of the input image affect the pixel value in the intermediate Laplacian pyramid $\{L[\tilde{I}]\}$ it is not necessary to compute all coefficients in the pyramid. Instead only a subregion is used. An even faster version of the algorithm, with similar performance, has been suggested [30]. That is achieved by precomputing a number of Laplacian pyramids and interpolating between their values based on the value of g.

2.5 Quality Assessment of Images

There are both subjective and objective ways of assessing image quality and contrast. In digital pathology what matters most is probably the subjective opinions of pathologists examining the images. However objective quantitative metrics can still

play a role in algorithm development and tuning. One widely used image quality metric is the structural similarity index [31]. This metric considers luminance, contrast and structure, all interesting characteristics in our application. However, the metric only accepts grayscale images and would thus require conversion to grayscale. Because the colour content of histopathology images is so important, the relevance is likely low.

One general purpose image quality assessment index extending to colour images is the Spatial-Spectral Entropy-based Quality (SSEQ) index [32]. SSEQ deals with the difficult problem to quantitatively score the quality of an image, without another image for comparison, i.e. a no-reference metric. For this the entropy of both spatial and spectral features are considered. It is training based and was trained on the LIVE IQA database. This database consists of images very different from digital pathology images including photographs of e.g. buildings, parrots and persons. A full description of the method is found in the original article [32]. Already at this point it should be emphasized that SSEQ is by no means designed for use within digital pathology but rather for natural scenes. The purpose including it was to investigate if it could be used for quality assessment of image enhancement in digital pathology.

Chapter 3

Aim

Pathologists are not always satisfied with the colours and details of digital pathology images. The overall aim of this work was to identify such problems and thereafter suggest image processing to solve one of them.

After consulting the literature and interviewing pathologists the focus area was chosen to be the display of mitotic figures. The choice was made due to the many clinical applications of knowing the presence and numbers of mitoses in a specimen.

No restrictions applied image processing algorithms to be explored, except that the contrast improvement technique CLAHE should be evaluated. The reason for including that specific algorithm beforehand was an interest from Sectra, the company supporting the thesis. The use of the algorithm is widespread and it is applied frequently in other medical imaging modalities.

Specific objectives for this work were:

- Identification of cellular structures that are troublesome for pathologists.
- Finding properties of and issues with hematoxylin-eosin digital pathology images.
- Examine CLAHE's effect on the display of mitotic figures.
- Suggest a suitable colour space for contrast adjustments of hematoxylin and eosin stained images.
- Explore other algorithms of use in digital pathology to facilitate the examination of mitotic figures.

The images were restricted to tissue stained with hematoxylin-eosin scanned at 40X, the standard magnification for examining mitotic figures.

Chapter 4

Methodology

4.1 Shortcomings of Digital Pathology Images

To identify cellular structures that often are misclassified and tasks that are tedious for pathologists the literature was studied. Moreover three experienced pathologists, using digitized slides in their daily clinical work, were interviewed.

4.1.1 Literature Review

The literature study (summarized in Table 4.1) focused on differences between what is seen in a light microscope compared to digital images of the same slides. It was necessary to distinguish between two types of problems; examinations being tricky both using a light microscope and digitally and tasks that are harder in the digital environment.

Before digital pathology was introduced in clinics a number of validation and feasibility studies were performed. The Department of Pathology at University Medical Center Utrecht has hosted several such studies. These were based on digital re-evaluation of old cases that originally had been examined in light microscopes. One hundred patients were considered in each study.

Table 4.1: Key findings of literature study.

Disadvantages of whole-slide images compared to light microscopy
• Harder to interpret mitotic figures. • The baseline magnification in the whole-slide images are often lower than the magnification that would be used in a glass microscope. • Microorganisms are small and thus hard to see in low magnification whole-slide images. • The visibility of nuclear details can be lower.

One feasibility study concerned gastrointestinal pathology [33]. 95 cases were concordant, meaning "complete agreement between the first original signed-out diagnosis and the diagnosis as drawn from the WSI". In the five non-concordant cases the digital diagnosis was more likely to be true in three out of five cases. It was observed that identification of microorganisms like *Candida albicans, Helicobacter pyroli* and *Giardia lamblia* was difficult using digitized slides. The mentioned microorganisms are a fungus, stomach bacterium and parasite, respectively. In the study it was concluded that 40X magnification would likely eliminate the problem. The slides in the study only used a baseline magnification of 20X.

A study regarding digital examination of breast tissue was done at the same institution [34]. In a case concerning a lumpectomy, a removal of a breast tumour and surrounding healthy tissue, the digital and conventional assessment agreed on primary histopathologic features whilst there was a difference in the scoring of immunohistochemical progesterone stainings.

Another research group found three discrepancies related to image quality [35]. One case concerned a bladder biopsy without visible umbrella cells on the epithelium in the digital images, resulting in thoughts of dysplasia. In the light microscope the nuclei were seen in more detail and no dysplasia was reported. A similar problem was reported with a skin biopsy. In both cases the focus was bad in the digitized slides.

In an article by Jukic *et al.* it was described that one pathologist experienced differences in distinguishing between urothelium and carcinoma *in situ* [36]. The first is the epithelial lining of the urinary tract and the latter a group of abnormal cells [37, p.162]. A possible explanation was suggested to be the restriction to 40X magnification in the digital slides.

It is hard for pathologists to interpret mitotic figures in whole-slide images [38], especially abnormal ones [39]. One explanation is their tiny size of mitoses [40]. In general the concordance among pathologists can be low when it comes to characterizing mitotic figures [41]. To assess if the lack of depth and limited fine-focusing in the digital images affect the possibility to identify mitotic figures, Al-Janabi *et al.* studied mitotic counts in breast tissue [42]. The study showed good agreement between mitotic counts in light microscopy examinations compared to whole slide imaging. Only a slight underestimation, without clinical relevance, occurred when mitotic figures were counted in digitized slides.

4.1.2 Interviewing Pathologists

To verify the findings from the literature review and identify other issues, three experienced pathologists were consulted. All were used to digital diagnostics. Table 4.2 gives a summary of the text.

Table 4.2: Key findings from interviews with pathologists.

Pathologist A	**Pathologist B**	**Pathologist C**
• Lack of nuclear detail in digital pathology images. • Important to preserve image brightness. • Important to preserve original colouring.	• Invisible chromatin pattern in digital slides. • Microorganisms are hard to see both digitally and in a microscope. • Recommendation to focus on a particular task. • Little lag is accepted.	• Mitotic figures can be identified by their prickly edges. • The cellular membrane of mitotic cells is informative. • Lymphocytes can be mistaken for mitotic figures. • Misses the button adjusting the amount of light.

The first pathologist expressed that in her opinion, the main shortcoming of the digital images was lack of nuclear detail such as distinctness of nucleoli. A wish that image processing should preserve the original brightness and colours was expressed.

The second pathologist experienced problems with the chromatin pattern in the nuclei in digital slides. This was mainly a concern in cytopathology, but also in histopathology. The problem with microorganisms found in the literature study was confirmed, although seeing such organisms was claimed difficult in light microscopy as well due to their tiny size. The suggestion in the feasibility study of simply scanning at 40X was refused as insufficient. In many cases 60X or higher magnifications might be necessary. During a second talk to this pathologist it was emphasized that whatever processing is applied, the chromatin pattern is not allowed to disappear. In neoplasms it may look like the chromatin is exploding in early stage mitoses. Moreover the mitotic figures often are non typical, such as tri- and quadripolar. This appearance is not found in healthy tissue. A piece of advise was to focus on some particular structure or task since general image enhancement was considered likely to fail. In addition little lag in the digital image viewer was accepted by this pathologist.

The third pathologist was interviewed regarding experiences of examining mitotic figures digitally. Two key issues to look for are diffuse prickly edges and that the suspicious mitotic figure is situated inside a cell. In practice though, it might be hard to see the cellular membrane. If this could be depicted more clearly, it could help in assessment of candidate mitotic figures. Besides, a risk of interchanging lymphocytes with mitoses was suggested. See the dark shape in the lower left corner of Figure A.1(k) in the appendix. Here it is hard to tell whether it is two lymphocytes in the epithelium or a mitotic figure. It was also expressed that pathologists often are non concordant regarding what is a mitotic figure and what is not. Melanoma and

breast cancer assessment were mentioned as two fields where mitotic counts are of particular interest. Since the applications of mitotic counts in melanoma were new to the author they were confirmed by [43].

In light microscopy the three-dimensional structure can be examined by adjusting focus back and forth. The digital counterpart with multiple focus planes was not considered very helpful, mainly due to the increased storage requirements. In a light microscope the "lighting-button" was used a lot. Digitally, the colour and contrast was changed in the viewer to increase perception. The pathologist had a clear view of how image enhancement of digitized slides should work. Enhancement was welcome as long as it could be turned on and off, and moreover the enhanced version should not replace the original if saved.

4.1.3 Conclusions from Litterature Study and Interviews

The outcome of the literature study was a bit sparse. Reported discrepancies between digital and conventional examinations were often based on a diagnose from an individual pathologist. Good focus is clearly essential throughout all regions of the image with clinically relevant tissue. However, this problem is out of the scope of this thesis since it is a scan-related problem. Lack of nuclear detail and difficulties with mitotic figures in whole-slide images were described in the literature and later confirmed in the interviews. At this point it was decided to focus on display of mitotic figures due to the high clinical value in cancer assessment.

Some remarks that should be considered during algorithm selection:

- Only small changes in chromaticity and overall brightness are likely to be accepted by pathologists.
- The chromatin pattern should not be destroyed, rather enhanced.
- Little lag is tolerated among pathologists. Hence, computational complexity should be considered.

4.2 Display of Mitotic Figures

To improve the display quality of mitoses it was first considered necessary to find differences between the pixels that represent a mitosis compared to those who not.

4.2.1 Image Database

To test image processing algorithms it is appropriate to use small snapshots of whole-slide images due to the size of the latter. Images with structures that possibly could be mitoses, hereafter referred to as candidate mitotic figures, were obtained in two different ways. The selection used the inclusion criteria:

- At least one candidate mitotic figure in the image.
- Hematoxylin and eosin staining.
- Scanned at 40X.
- Bitmap (.bmp) format.
- 1024 x 1024 pixels

A number of images from breast tissue were selected from the MITOS dataset [44], with permission of the copyright owners. This dataset was originally created for a pattern recognition competition on automatic counting of mitoses in 2012 [45]. One benefit with this dataset is that it contains snapshots of whole slides scanned both with Aperio ScanScope XT and Hamamatsu NanoZoomer 2.0-HT scanners. Different scanners may yield different colours and thus it is of interest to include scanners from several manufacturers. In addition, images look differently from lab to lab depending on the composition of stains and processing.

Images with candidate mitotic figures were also selected from whole-slide images scanned at 40X. Clinically relevant images were selected to easier attract pathologists' attention when asking for their opinion. To ascertain clinical relevance, a senior pathologist judged the image set from a mitosis-assessment viewpoint. The images represented some of the variation usually observed in hematoxylin-eosin images, ranging from almost completely pink with high affinity for eosin to purple with high affinity for hematoxylin. One snapshot with plenty of background and fat, appearing white, was included to investigate how the algorithms coped with unstained homogeneous image regions. Some of the images are from tissue unknown to the author due to anonymization. Both the manually selected images and those from the database are found in Appendix .

Bitmap format was used to avoid artefacts that may arise when processing images compressed with lossy techniques such as JPEG (.jpg). Since CLAHE divides images into smaller tiles a fixed size of 1024 x 1024 pixels was chosen since it is evenly divisible with an even number of tiles and large enough to be clinically relevant.

4.2.2 Image Statistics

A few snapshots of mitoses were taken from hematoxylin and eosin stained slides at 40X magnification. These were converted to the L*a*b* colour space to compute histograms for the L* channel of the full image, parts displaying a mitosis and the background. This yielded information (cf. Section 5.1) that was incorporated in algorithm selection and tuning.

4.2.3 CLAHE in HSV and L*a*b* Colour Spaces

Since one of the aims of this work was to evaluate the effect of CLAHE on digital pathology images, it was the first algorithm considered. Hence a colour space to work

in and what channel(s) to apply CLAHE to had to be decided. Since interviewed pathologists were not willing to accept large changes in chromaticity, colour spaces where the intensity and chromaticity are separated were used. L*a*b* is designed to be perceptually uniform and hence a good candidate for histogram processing. HSV also separates colour from luminance. An advantage of these colour spaces are the available conversion functions in image processing software and libraries such as MATLAB [23], OpenCV [46] and Scikit-Image [47].

To determine if roughly the same clip limit and number of tiles could be used for most images, various settings were tested. The clip limit was restricted to avoid large changes. If the MATLAB implementation of CLAHE (`adapthisteq`) was used, the normalized clip limit was typically set in the range 0.01 (default) - 0.001. The possible range is [0, 1] where 1 corresponds to adaptive histogram equalization as explained in Section 2.4.3. The same number of tiles were used in horizontal and vertical direction. Working with images of size 1024 x 1024 pixels and using 8 x 8 tiles, the size of each tile is 128 x 128 pixels. Hence the actual clip limit obtained from a normalized clip limit of 0.001 is 80 (cf. (2.8)). If instead 16 x 16 tiles are used the clip limit is scaled proportionally to 20 (75% area reduction).

Processing in L*a*b* compared to HSV seemed to yield images with brighter colours. To compare objectively, CLAHE was applied to all twelve images in the dataset using a normalized clip limit of 0.001, 16 x 16 tiles and 256 bins. This was done both in HSV and L*a*b*. If applying CLAHE in the two colour spaces would result in similar brightness, the mean values of the RGB channels should be similar after processing. For assessment, two-sided paired t-tests of the pairwise differences between the means were carried out. The red, green and blue channels were tested independently at 5% significance level. To exemplify, the twelve mean values of the red channels of the images after processing in L*a*b* were compared to the corresponding mean values after processing in HSV. In addition, SSEQ scores of the original and enhanced images were computed.

In general CLAHE resulted in darker images. To preserve the original brightness the following approach was considered. The mean intensity values of the original and enhanced images were computed. The intensity of the enhanced image was thereafter scaled by the means ratio. Denoting the original mean $\bar{L}^*_{\text{original}}$ and the intermediary enhanced mean $\bar{L}^*_{\text{enhanced}}$, the new intensity value $L^*_{\text{new}}(x, y)$ was computed as

$$L^*_{\text{new}}(x, y) = \frac{\bar{L}^*_{\text{original}}}{\bar{L}^*_{\text{enhanced}}} L^*(x, y). \tag{4.1}$$

Here $L^*(x, y)$ is the luminosity after CLAHE of the pixel positioned at (x, y). Any output intensities outside [0, 100] range were set to the minimal and maximal intensities, respectively. Only the latter had to be applied. Note that the suggested procedure does not result in identical original and enhanced means if there are pixel saturation.

Other attempts of obtaining satisfying image brightness by modifying CLAHE was done. The redistribution of pixel values in CLAHE can be confined to the original

range of the input image. In that fashion values lower or higher than the original extremes are avoided in the enhanced image.

A uniform target distribution is mathematically the way to obtain maximal contrast in adaptive histogram equalization. If other target distributions are used it is called histogram specification instead of histogram equalization [20, p.94]. Some images were processed with a Rayleigh target distribution, i.e. using the probability density function [48, p. 95]

$$p(x) = \frac{x}{\sigma^2} e^{-\frac{x^2}{2\sigma^2}}, \quad x > 0. \tag{4.2}$$

Here the user defined parameter σ offers possibilities to tune the target distribution. Thereby the CLAHE output could be shifted towards higher intensities to avoid darkening, in particular of mitotic figures. In Figure 4.1 a Rayleigh distribution on the interval [0, 1] is depicted with $\sigma = 0.7$. Using such a target distribution in general shifts the intensities towards higher values.

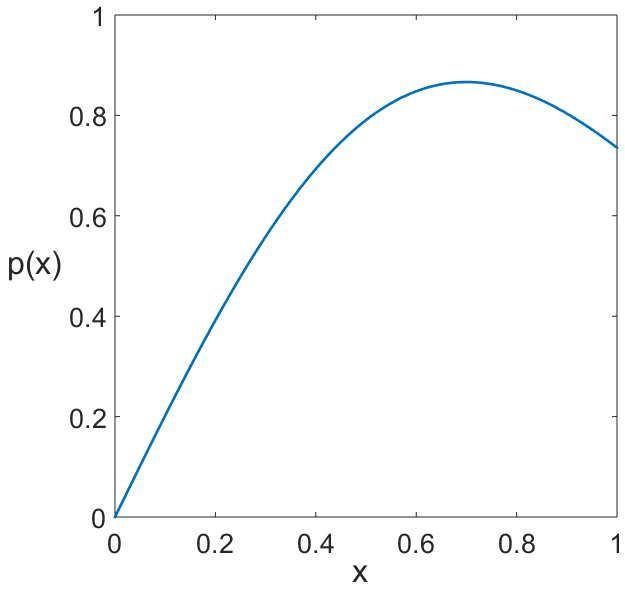

Figure 4.1: Rayleigh probability density function using $\sigma = 0.7$

4.2.4 Colour Deconvolution

To improve the contrast of mitotic figures and nuclear details it might be both unnecessary and counterproductive to process the tissue stained with eosin. Nuclei have high affinity for hematoxylin and thus end up purple. Therefore a combination of colour deconvolution and contrast adjustment of the hematoxylin channel was suggested, to improve the visibility of the nuclear details such as nucleoli, chromatin pattern and most important mitotic figures. To the author's knowledge, the combination of colour deconvolution and applying CLAHE to the hematoxylin channel is novel. The colour deconvolution followed the steps in Section 2.4.4. First all values

of the original RGB image were normalized to the interval [0, 1]. Thereafter the optical density image was computed by taking the negative of the base ten logarithm of the normalized RGB image. The colour deconvolution matrix was obtained as the inverse of the stain matrix. Finally matrices representing the amount of the different stains were found.

The matrix with hematoxylin saturations was first normalized to $[\epsilon, 1]$, with $\epsilon = 10^{-5}$. The small value ϵ was used instead of 0 for numerical reasons, because $\log_{10}(0) = -\infty$. CLAHE was subsequently applied to the hematoxylin channel whereafter scaling back to the original range was done. Finally the hematoxylin, eosin and residual channels were recombined into an RGB image by inverting the operations in (2.11) and (2.10). This is done by multiplying the stain matrix with the new stain saturation $\mathbf{v}_s^*$ vector where the first element has been modified by CLAHE to obtian the new optical density vector $\mathbf{v}_{OD}^*$.

$$\mathbf{v}_{OD}^* = \mathbf{V}\mathbf{v}_s^* \tag{4.3}$$

Finally the optical densities are converted to the original RGB space

$$\mathbf{r}^* = 10^{-\mathbf{v}_{OD}} \tag{4.4}$$

where $\mathbf{r}^*$ are the normalized RGB values of the output pixel. In the colour deconvolution plugin [49] in the image processing software ImageJ [50], there are two suggestions of colour matrices for deconvolution of hematoxylin-eosin images into the three components hematoxylin, eosin and residual. Due to the variation in the images it was questioned how well these general matrices can work. The first suggested colour matrix is

$$\mathbf{V}_1 \approx \begin{bmatrix} 0.64 & 0.093 & 0.64 \\ 0.72 & 0.95 & 0.0010 \\ 0.27 & 0.28 & 0.77 \end{bmatrix}$$

and the second is

$$\mathbf{V}_2 \approx \begin{bmatrix} 0.49 & 0.046 & 0.76 \\ 0.77 & 0.84 & 0.0010 \\ 0.41 & 0.54 & 0.65 \end{bmatrix}.$$

In the matrices the first column corresponds to the normalized optical density of hematoxylin, the second eosin and the third the residual.

A script for calculation of stain vectors from user-selected regions was constructed. Regions of interest were placed on areas having high affinity for eosin and hematoxylin, respectively. The third vector could be selected from a region of interest placed on the gray background or computed as the cross-product of the two other vectors to ascertain orthogonality and thus better represent actual errors. Instead of incorporating the residual vector one could work only with the physical hematoxylin and eosin vectors. Then one need to calculate the pseudo-inverse to obtain

the deconvolution matrix **D**. If the residual vector is included it is possible to get an estimate of the error using the norm of the residual channel. To quantify the errors, the mean square error ϵ_{MSE} was computed from the residual channel matrix **R** as

$$\epsilon_{\text{MSE}} = \frac{1}{M \cdot N} ||\mathbf{R}||^2 \tag{4.5}$$

assuming an image with M rows and N columns.

Besides CLAHE a simpler approach for enhancing hematoxylin rich structures was considered. Nuclei have some affinity for eosin although they are mainly stained by hematoxylin. Therefore the eosin and residual channels were scaled down to obtain an image with more prominent hematoxylin stain.

4.2.5 Unsharp Masking

Sharpening with unsharp masking was considered for two reasons. First it is a good reference technique as it has been used for long in digital pathology. It is applied already at scan time in some scanners. Secondly, sharp edges of mitotic figures were thought to be helpful for pathologists in their examination. Once again the colour space is important. As with CLAHE, the usual way of sharpening a colour image is to process the intensity channel only. Here the L* channel in L*a*b* was used. Blurring was done with Gaussian filters of varying width and the gain factor k varied between 0.5-2.

Since the luminosity is processed, sharpening can be integrated efficiently in a processing scheme where CLAHE is applied first to improve the contrast and unsharp masking second to increase the visibility of details and edges. The reverse order of applying the algorithms was also considered.

To enhance the details of mitoses it is questionable to process the whole slides due to their size. Hence region of interest based sharpening was applied to some images. Regions of interests were placed on mitotic figure candidates whereafter unsharp masking was applied to the selected regions. In the clinical setting this could be helpful since most mitoses are not that hard to examine. Therefore it makes sense to only apply image processing to specially difficult cases.

4.2.6 Local Laplacian Filtering

Detail enhancement using local Laplacian filtering was an attempt to use the pyramidal format for more than fast rendering. The edge-aware method could possibly leave the blurry edges of mitoses unchanged and instead enhance the details within mitotic figures with loose chromatin and of surrounding cytoplasm.

Paris and colleagues [27] kindly provided source code of their implementation of local Laplacian filters. The Gaussian and Laplacian pyramids used ten different scales

ranging from the baseline 1024 x 1024 RGB input image to the top of the pyramid of size 2 x 2. As remapping function, the one suggested for detail enhancement in the original article was used, see (2.13).

To identify good parameter settings all images in the dataset were subject to processing. There are a number of parameters; σ used to distinguish edges from details and α and β in the remapping function. Good values of σ stretched from approximately 0.1-0.4 depending on how colourful the image was. If colours are changing rapidly between different local regions more pixels will be considered as edges due to the increased distance in RGB space. α should be tuned to balance detail enhancement but avoid too much amplification of noise. β affects the mapping for pixels considered as edges. Values of β above one amplify edges, which might be useful for images from the MITOS dataset. In these bright pink breast tissue images the edge amplification can make the darker mitotic figures pop-out.

4.2.7 K-means Clustering

The colour deconvolution technique for histopathology images was originally developed to quantify the amount of stain in pathology images. For display-enhancement purposes it was realized that simple k-means clustering could be used to achieve a cluster containing nuclei pixels to which image processing could be applied. The main difference with this approach is that a pixel is determined to fully belong or not belong to the nuclei cluster. With colour deconvolution only a part of the pixel's colour is found on the hematoxylin channel.

K-means was applied with three clusters to yield one cluster with purple structures, one with pink and one with background. Input features from each pixel were the chromaticity channels of its L*a*b* representation, the a^* and the b^* values. The Euclidean norm was used for the objective function in (2.12). The cluster with bluish pixels were subject to CLAHE by applying the algorithm to an image with the pixels in the blue cluster mounted on a black background. For this the corresponding L^*-values were processed. The intuition was that the black background should fill the lower intensity range in the CLAHE remapping, yielding brighter nuclear details. Finally, the pixels in the blue cluster of the original image were replaced with the processed correspondence.

4.3 Validation with Pathologist

For validation, an image scoring test with a pathologist took place.

4.3.1 Test Session Format

A senior pathologist was asked to score a number of images with respect to the following criteria:

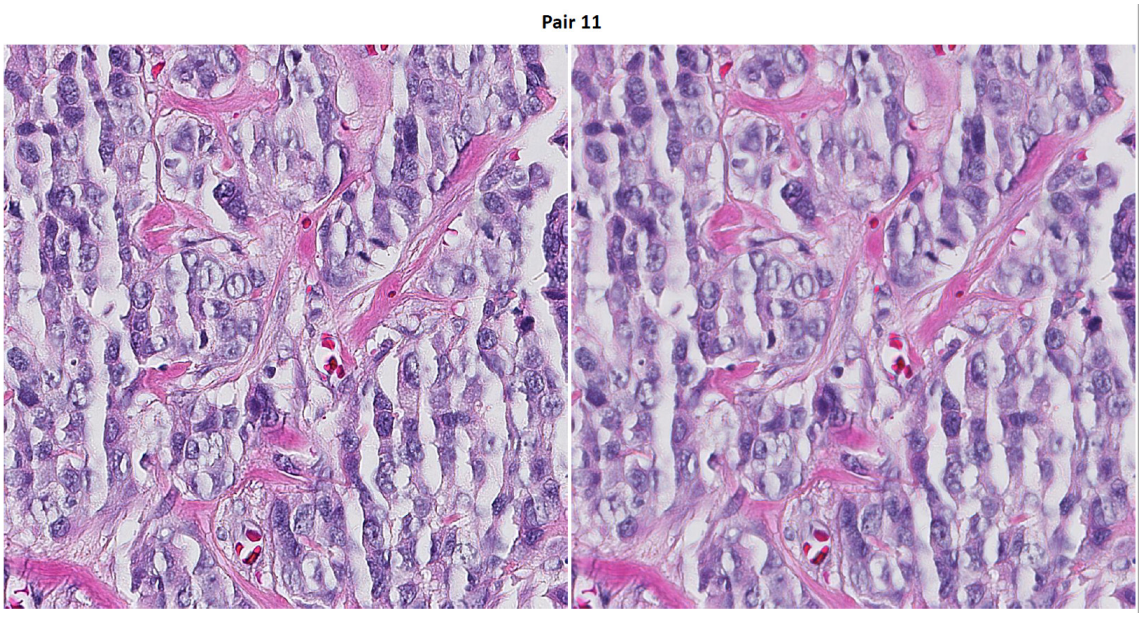

Figure 4.2: One image pair in the test with unsharp masking (left) and the original (right).

- Details of candidate mitotic figures.
- Overall image quality.

The first criterion reflects the direct aim of the thesis. The reason that *candidate* is included in the description is due to the difficulties of telling whether or not suspicious mitotic figures in the set of images really are mitoses. The second criteria was included to make sure that the colours and noise level in the images were not affected too much by the image processing.

Images were presented pairwise in Microsoft Powerpoint. Each pair included an original image and a processed version. For each pair the images were first displayed next to each other as in Figure 4.2 and thereafter one by one. The scoring was based on pairwise similarity judgements where the pathologist was asked to compare the right image in the pair to the left one according to the criteria above. The answers were given by marking check-boxes on a paper form with the rankings *much worse, slightly worse, same, slightly better* and *much better*. The pathologist was not told which image that was processed. Moreover, the original and processed images occasionally flipped sides. When each pair had been showed two pairs re-appeared to check if they would obtain the same result the second time.

The images used in the test were the set of images in Appendix . The order of the images were manually selected, trying to achieve a spread of the images and the different algorithms. It was considered a priori that for significant conclusions a larger set of images could be needed. But with a single referee it was considered most important to only show images of clinical interest. Two contrast adjustment techniques, CLAHE and local Laplacian filters, and sharpening with unsharp masking was tested. The combined approach with colour deconvolution and CLAHE was

left out due to difficulties with obtaining good stain vectors for all images.

The evaluated image pairs were:

- 12 pairs with CLAHE-L*a*b* images and originals.
- 12 pairs with local Laplacian filtered images and originals.
- 12 pairs with images sharpened with unsharp masking and originals.
- 2 pairs occurring at the end from the above mentioned to examine if the referee was consistent.

For the different algorithms fixed parameter values were used for all images. CLAHE used 16 x 16 tiles, a normalized clip limit of 0.001 and 256 bins in the remapping function. The algorithm was applied to the L^* channel in L*a*b* and the target distribution was uniform. The clip limit was low to avoid too drastic output changes.

The local Laplacian filtering was done with $\sigma = 0.2$, $\alpha = 0.4$ and $\beta = 1$. The images of breast tissue from the MITOS dataset are more pale and homogeneous than the other images. They were visually less affected by the local Laplacian filters than the other images.

The unsharp mask used a 9 x 9 Gaussian filter for blurring and $k = 1.5$. This is a considerable amount of sharpening in this application. The elements of the Gaussian filter h summed to one, i.e. $\sum_{i=0}^{8}\sum_{j=0}^{8} h_{ij} = 1$, to avoid saturation problems and keep homogeneous regions unchanged.

4.3.2 Statistics

After the test, 38 pairwise rankings were available, twelve for each algorithm and in addition two reappearing pairs. The possible answers were transferred to a numeric ordinal scale by assigning values to these,

- -2 *much worse*
- -1 *slightly worse*
- 0 *same*
- 1 *slightly better*
- 2 *much better*

Hence positive scores meant improvement of the mitotic display or general image quality, according to the pathologist. If the enhanced and original images were just as likely to be considered better, a zero median is reasonable using the ordinal scale. For the three evaluated algorithms two-sided sign tests where carried out to test for zero median and an alternative hypothesis of median different from zero. Refusing the null hypothesis thus means effect in either direction of the image processing.

The level of significance was set to 95 %. A good description of the sign test is found in [51, pp.118-122] which is summarized here.

The null hypothesis H_0 of median $m_0 = 0$ versus an alternative hypothesis H_1 of $m_0 \neq 0$ can be tested by considering signs. For each algorithm and criterion, $N = 12$ scores $X_1, X_2, ...X_N$ are available. The sign of all X_i's greater than zero is '+' and the sign of all X_i's less than zero is '-'. Cases were $X_i = 0$ are neglected. Let T be the number of positive signs

$$T = |\{i = 0, 1..., N;\ X_i > 0\}|. \tag{4.6}$$

If H_0 is true then $T \sim Bin(n, 1/2)$ where $n = N - u$ and u is the number of ties. Let α be the level of the test. Given T, critical values are integers less or equal to $t^{\text{low}}_{\alpha/2}$ or greater or equal to $t^{\text{high}}_{\alpha/2}$. $t^{\text{low}}_{\alpha/2}$ is the smallest integer for which

$$\sum_{t=0}^{t^{\text{low}}_{\alpha/2}} \binom{n}{t} (\frac{1}{2})^n \leq \alpha/2 \tag{4.7}$$

and $t^{\text{high}}_{\alpha/2}$ is the largest integer for which

$$\sum_{t=t^{\text{high}}_{\alpha}}^{n} \binom{n}{t} \left(\frac{1}{2}\right)^n \leq \alpha/2. \tag{4.8}$$

Finally the p-value, the probability of observing T or a more extreme result assuming that H_0 is true is computed

$$p = \sum_{i=0} n - T' \binom{n}{i} 2^{-n}, \quad T' = \min\{T, n - T\} \tag{4.9}$$

In [51, p.122] it is suggested to randomly assign tied values a sign. Due to the small sample sizes, the alternative approach of neglecting ties were chosen.

4.3.3 Quantitative Validation

Initially the purpose of incorporating the SSEQ index was to determine if there is any correlation between the quality estimated by the index and a pathologist. Whilst assessing the quality of images processed with CLAHE in L*a*b* and HSV the index had appeared to be informative. However, after observing unsatisfying behaviour of SSEQ for several images this was changed. In Figure 4.3 an example is given where adaptive histogram equalization has ruined the original image. Yet it is claimed to be of better quality according to the SSEQ index. Therefore the index was not used for more testing.

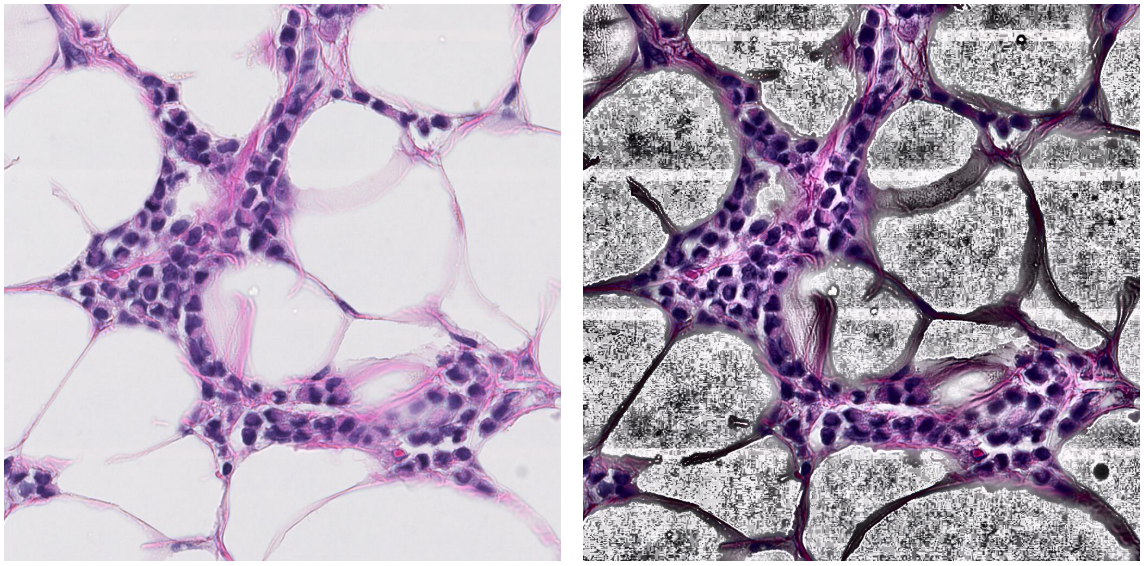

(a) Original image. SSEQ 34.43

(b) Severly distorted image after adaptive histogram equalization. SSEQ 11.13

Figure 4.3: SSEQ is unreliable for pathology images. In (b) adaptive histogram equalization has been applied and the image obtains a lower score than (a), indicating better image quality, even though it is useless for a pathologist.

4.4 Implementing CLAHE in Sectra's Pathology Viewer

Processing snapshots from digital slides can be useful whilst evaluating different algorithms. Nevertheless, for clinical use the algorithms need to be available in the software used to view the digital slides. At an early stage of this work CLAHE was added as a functionality to Sectra's viewer for digital slides. This was a sidetrack of the more issue-oriented work described earlier which focused on display of mitoses. Since CLAHE is so general it was assumed to be useful, even though not for enhancing mitotic figures.

Sectra's viewer is a web application connected to a picture archiving and communication system on a server. The displayed part of the digital slide is retrieved in smaller tiles from the server and thereafter merged to create the field of view.

In the CLAHE implementation all image processing was carried out on the server. The server was a local virtual machine running Windows Server 2012 R2. The virtual machine was a 64 bit system with dual processor cores and 2048 MB memory. For the virtual environment VirtualBox was used. The CLAHE implementation in EmguCV was used [52]. It is a wrapper of OpenCV to .NET. Processing was done on the L* channel in L*a*b* representation. If the tiles would be processed individually at retrieval severe boundary-artefacts would occur. Therefore nine tiles were required for each individual tile to be retrieved. Approximately 25% overlap between the middle tile and the others was used as illustrated in Figure 4.4. CLAHE

was applied to the padded centre tile, whereafter the latter was sent from the server to the client. On the client a CLAHE-button was added (cf. Figure 4.5). The button determined the value of a boolean flag, deciding whether CLAHE should be applied or not when tiles were retrieved from the server.

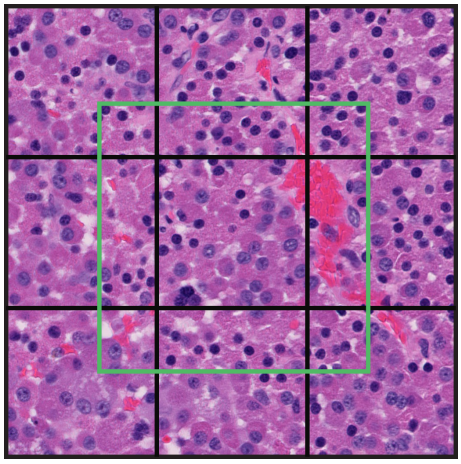

Figure 4.4: CLAHE is applied to the region within the green square. Thereafter the middle tile is retrieved from the server.

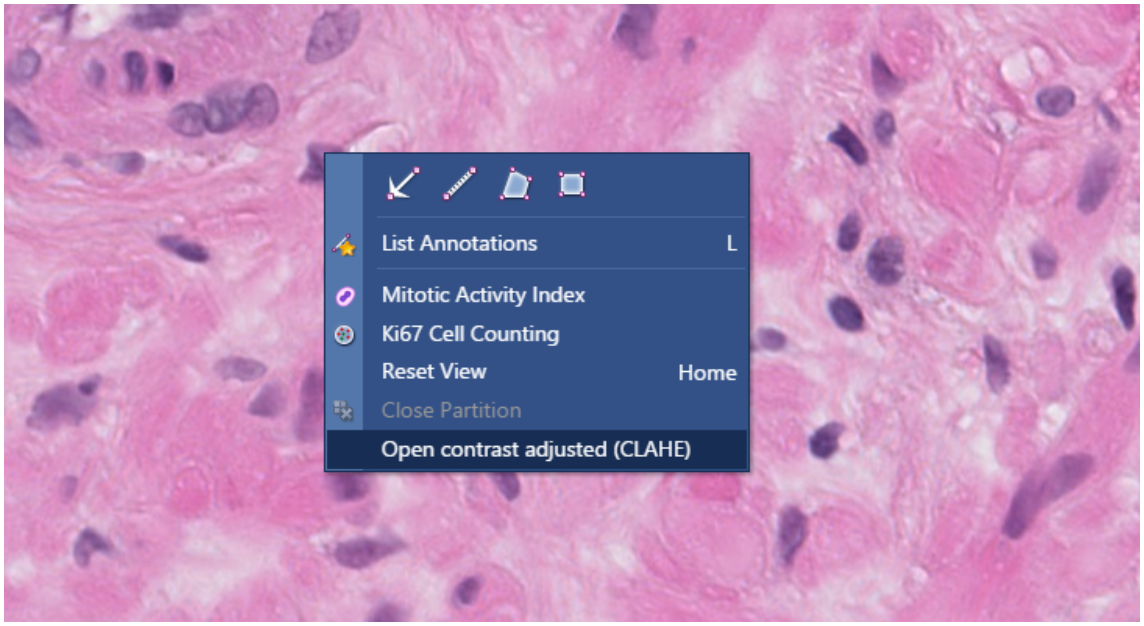

Figure 4.5: CLAHE button in Sectra's viewer.

The implementation was intended as a prototype. Limited attention was paid to usability. When the user pressed the CLAHE button in a menu a second window was opened showing the same view but with CLAHE applied. The two-side view was synchronized so that when one navigates in one window the view in the other follows. The number of tiles in x- and y-direction and the clip limit of CLAHE were fixed without user input. No clinical tests of the implementation was done

since CLAHE showed low potential for enhancing the display of mitotic figures as described in the next chapter.

Chapter 5

Results

A number of different techniques have been evaluated. Besides the quantitative results from the validation session with the pathologist and computations of SSEQ scores, this chapter contains observations. These shall not be seen as validated truths, the purpose is rather illustration of different results. The images used in the illustrations are cropped to outline mitotic figures. Seeing the details of mitoses is otherwise difficult in small images.

5.1 Image Statistics

An interesting finding from the calculation of histograms of mitoses and surrounding tissue was that mitoses tend to populate lower intensities. Typically the L* values of the mitotic figures are i the range 5-40. Example histograms of snapshots with mitoses and background (surrounding tissue) are depicted in Figure 5.1 and 5.2. In the top right histograms of the full images the mitotic intensities are drowned due to their lower numbers.

5.2 Results of Different Algorithms

The evaluation of the different algorithms is based on comparisons with the original images. The algorithms have not been compared against one another.

5.2.1 CLAHE in HSV and L*a*b*

CLAHE improved the global contrast but showed less success in enhancing the mitotic figures. The drawbacks were darkening of non-mitotic image regions and increased size of mitoses. When other structures become just as dark as the mitoses, the pop-out effect of the mitotic figures is destroyed. Moreover the marker mitotic figures appeared to reduce the visibility of details. When CLAHE was applied the

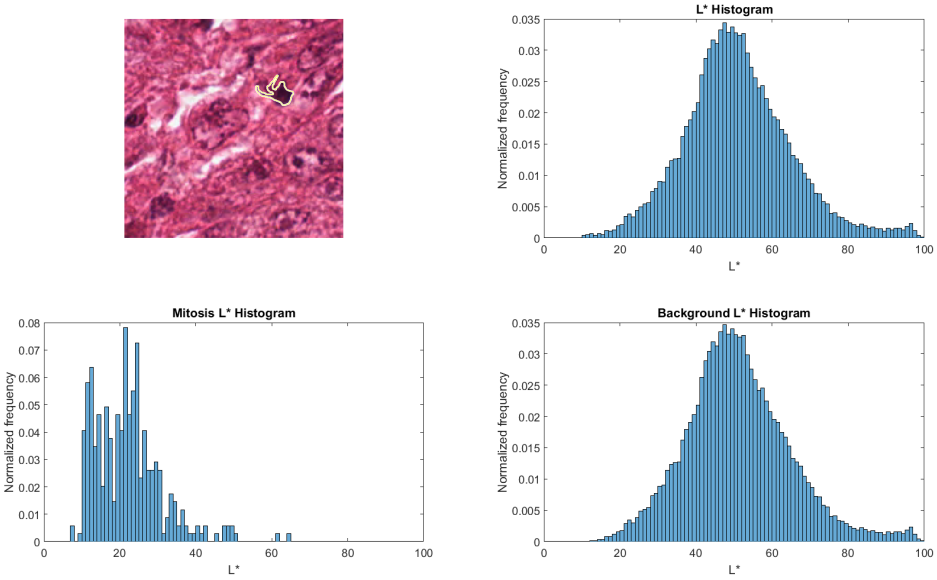

Figure 5.1: A mitosis and corresponding histograms. The yellow line encompasses the mitosis.

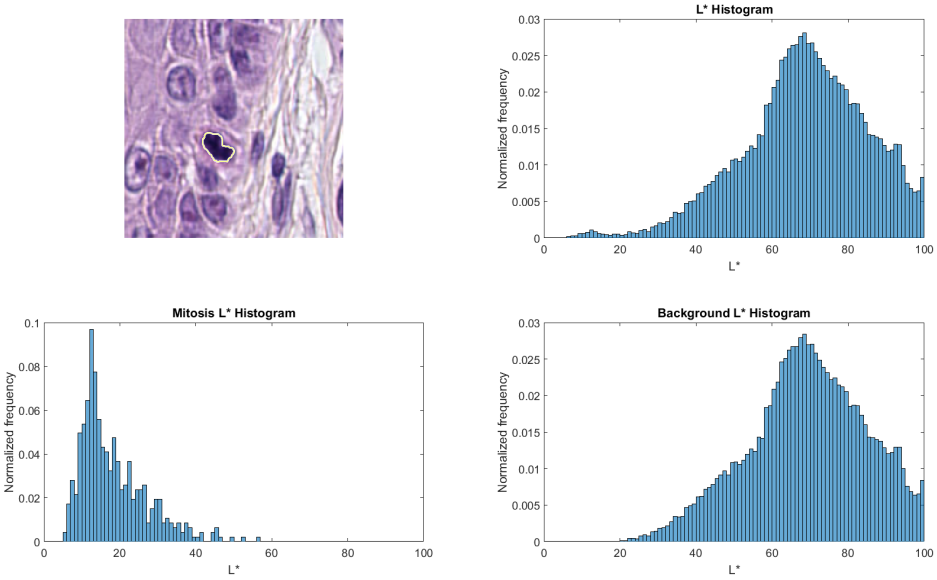

Figure 5.2: Another mitosis and corresponding histograms.

normalized clip limit was set to low values to limit the change of the overall image appearance. As illustrated in Section 5.1 high intensities are more common than lower ones in many hematoxylin and eosin images. Therefore histogram equalization and modifications resulted in darker images in general. In Figure 5.3 an unprocessed and image enhanced with CLAHE are shown. When low normalized clip limits are used as in this case the darkening of the background is limited. Apparently the nu-

clear details appear with more contrast in Figure 5.3(b) than 5.3(a). Unfortunately the candidate mitotic figure grows as a result of CLAHE.

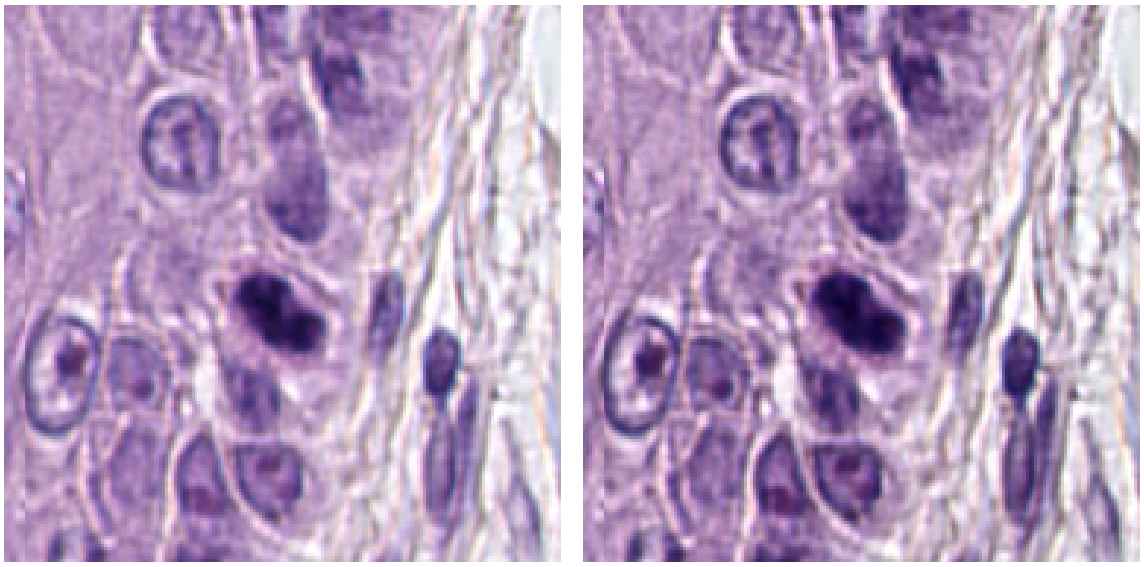

(a) Original image of skin.

(b) CLAHE with normalized clip limit of 0.001, 16 x 16 tiles and 256 bins.

Figure 5.3: Candidate mitotic figure that might be two lymphocytes.

For most hematoxylin-eosin images the number of tiles did not affect the output much if the same normalized clip limit was used. This was true as long as the snapshots had rougly similar characteristics in all regions. Regarding the number of bins used to calculate the mappings, a higher number increases the dynamic range. Increasing the number of bins did not always result in visual improvements.

Applying CLAHE in L*a*b* compared to HSV might increase the visual colour contrast slightly. The difference between the two increased with the normalized clip limit. For the paired t-tests, H_0 was refused for the red and blue channels indicating unequal mean values between the images processed in the colour spaces. For the green channel H_0 could not be rejected with high p-value as shown in Table 5.1.

Table 5.1: Paired two-sided t-test for means of the twelve images processed in L*a*b* and HSV at 95 % significance level.

Channel	Decision	p−value
Red	H_1	$p < 0.05$
Green	H_0	$p = 0.89$
Blue	H_1	$p < 0.05$

In Table 5.2 the SSEQ values of the twelve images in the dataset before and after CLAHE in L*a*b* and HSV colour spaces are given. The scores were rounded to one decimal. Interestingly all scores for the images where CLAHE was applied to the V

channel of the HSV representation are slightly higher than the L*a*b* counterpart. Remember that a higher SSEQ score indicates a lower image quality. The original images' scores are sometimes higher and sometimes lower than the contrast enhanced correspondence.

Table 5.2: SSEQ of original images and after CLAHE in L*a*b* and HSV.

Image	1	2	3	4	5	6	7	8	9	10	11	12
Original	29.7	51.1	34.4	56.8	49.3	47.2	49.8	40.1	43.6	37.5	31.4	33.7
HSV	30.2	52.3	33.1	56.9	50.7	48.38	52.2	40.9	43.9	37.6	31.7	34.5
L*a*b*	29.9	50.6	31.5	54.7	48.5	47.0	50.3	39.7	43.8	37.3	30.5	33.3

To combat the darkening of images the brightness preservation procedure outlined in (4.1) was considered. The result was not always satisfying. Many pixels reached and exceeded the upper saturation limit $L^* = 100$ in resulting in too distorted output.

With a Rayleigh target distribution, the shape of the distribution could be tuned using the σ parameter. Thus making the overall image darker could be avoided. This is illustrated in Figure 5.4. Here CLAHE used a clip limit of 0.005, 32 x 32 tiles and 256 bins. The parameter σ was set to 0.7. Nevertheless, it was impossible to find general settings working well for different images.

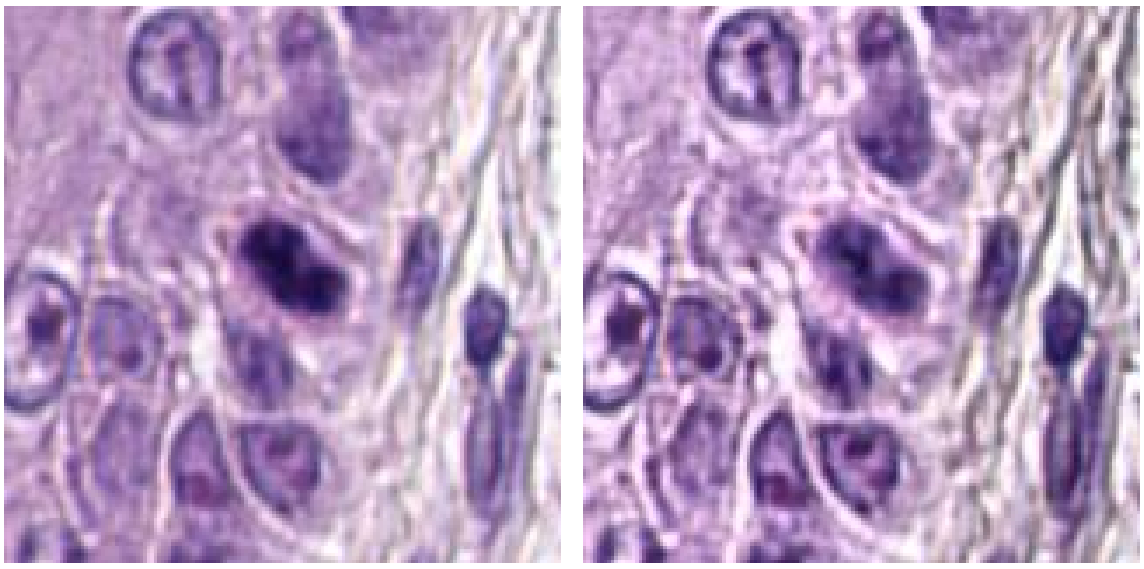

(a) Original image

(b) CLAHE with Rayleigh target distribution.

Figure 5.4: Example using histogram specification in CLAHE.

5.2.2 CLAHE and Colour Deconvolution

The novel combination of colour deconvolution and CLAHE improved the contrast of nuclei in relation to surrounding tissue. Nuclei, including nucleoli and chromatin patterns became more visible. This is illustrated in Figure 5.5. Here CLAHE used a normalized clip limit of 0.002, 256 bins and 16 x 16 tiles. It should be noted that the parts of image mainly stained with eosin are affected as well. Regarding mitotic figures, these tended to end up both larger and darker similar to when CLAHE was applied in L*a*b* and HSV.

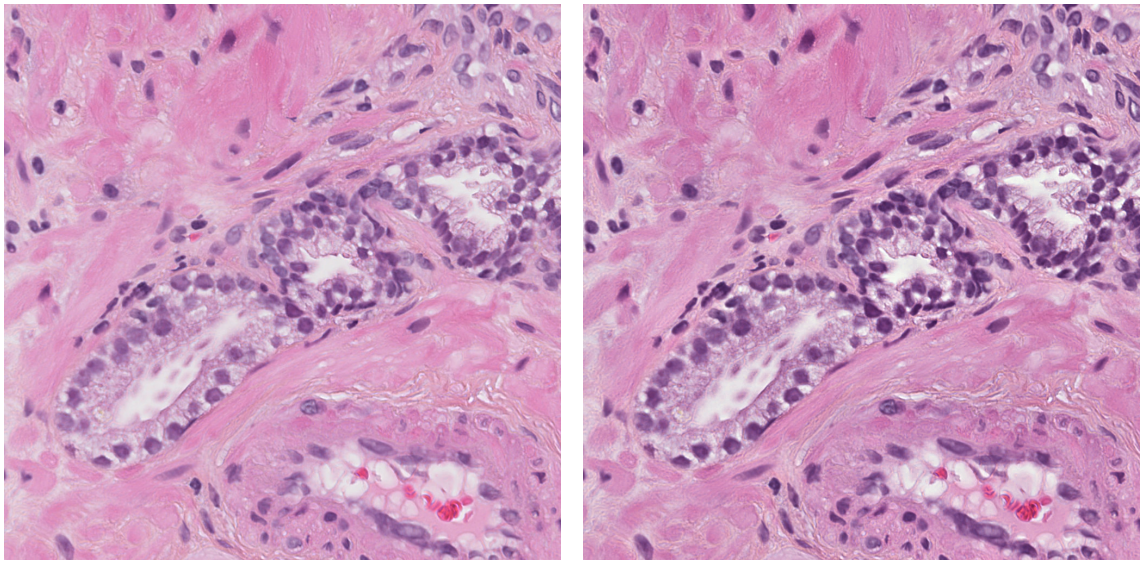

(a) Original image

(b) After colour deconvolution and CLAHE of hematoxylin channel.

Figure 5.5: Comparison of image from a prostate biopsy before and after colour deconvolution and CLAHE of hematoxylin channel.

The operation showed to be risky, especially in background regions, where the colours sometimes ended up distorted. The effect could be dramatic changes of e.g. the background which turned bright blue in some cases. In Figure 5.6 the same image has been subject to CLAHE (clip limit 0.002, 8 x 8 tiles, 256 bins) but using the two different stain matrices in Section 4.2.4. In the first case, where the background is distorted, ϵ_{MSE} was 0.024 compared to $1.88 \cdot 10^{-4}$ in the second case. This indicates that inadequate deconvolution may result in strange effects after processing. Here it should be emphasized that the colour matrices adopted from ImageJ were not measured on the same scanner and stain combinations as the image. This illustrates the importance of the stain matrix.

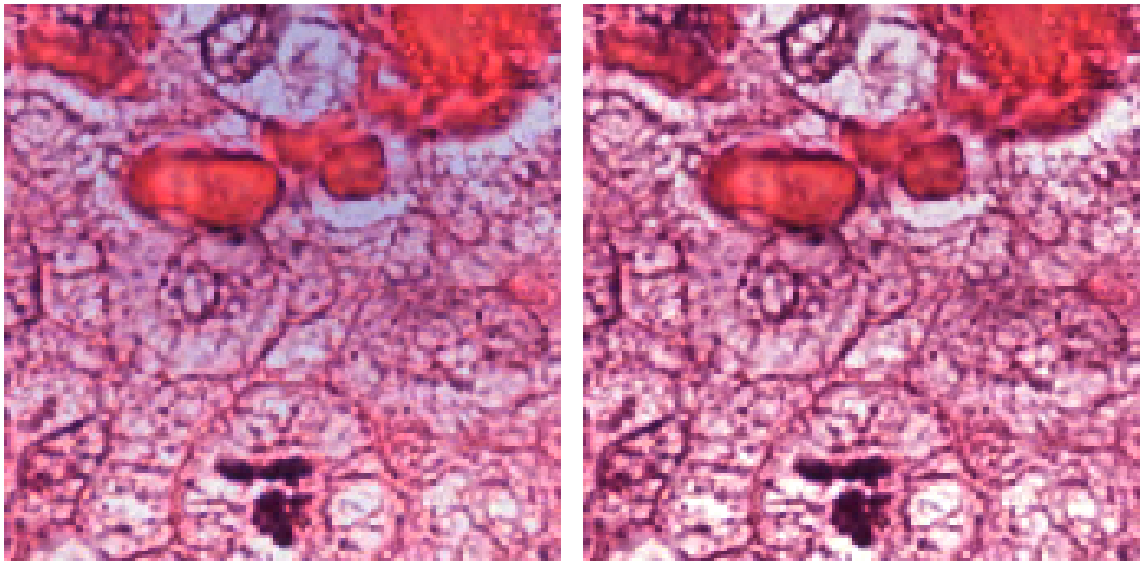

(a) Using stain matrix $\mathbf{V}_1$. (b) Using stain matrix $\mathbf{V}_2$.

Figure 5.6: Results after CLAHE using different stain matrices.

Determining the stain matrix from regions of interest worked well when the image contained parts where it was reasonable to believe that almost all colour was caused by a single stain.

The simple approach of simply scaling down the elements of the eosin and residual matrices yielded expected results. Nevertheless, the display quality of mitotic figures remained the same. For messy images with huge amounts of stain such as A.1(g) it might be a useful, since the original amount of eosin is very high.

5.2.3 Local Laplacian Filters

Local Laplacian filtering could be applied directly to the RGB image without distorting the colours considerably. The filters showed to be very general since the parameters offer a lot of tuning possibilities.

The effect of local Laplacian filters varied for mitoses in different stages. Small dense mitotic figures were not affected much. Mitotic figures in metaphase, such as the one in the lower right part of Figure A.1(a), were almost unaffected. For mitoses in phases where the chromatin is less dense, such as prophase (cf. Figure 5.7(c)) and anaphase (cf. Figure 5.8(c)), the results were better. In these cases it was easier to see the localization of the chromatin compared to the original images in Figures 5.7(a) and 5.8(a), respectively. In the second example the cell membrane between the separating nuclei became more distinct. Unfortunately, detail enhancement of the full snapshots sometimes resulted in emphasizing irrelevant structures in the cytoplasm.

5.2.4 Unsharp Masking

Sharpening with unsharp masking yielded visually attractive results as long as the amount of sharpening was moderate. When the gain k and the radius of the Gaussian filter were increased, noise became over-amplified. In Figures 5.7(d) and 5.8(d) the edges within the mitotic figures are sharper, resulting in improved visual contrast compared to the originals in (a). On the other hand the background becomes less smooth.

Sharpening only the regions including mitoses results in one major concern. If a nice region is selected such as a square it is easy to deal with the boundaries through standard reflection when the unsharp mask is applied. If on the contrary only the mitosis is selected, treating the boundaries becomes very tricky.

When CLAHE and unsharp masking was combined it resulted in sharper and contrast adjusted images, but the size of the mitotic figures still increased. The order in which the algorithms were applied was not as important as expected. Sharpening both before and after after contrast-adjustment worked.

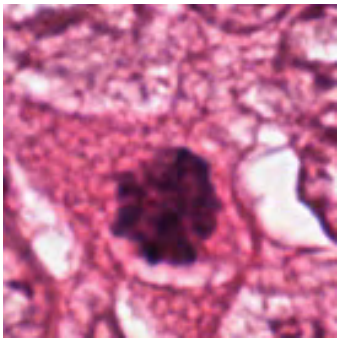

(a) Original

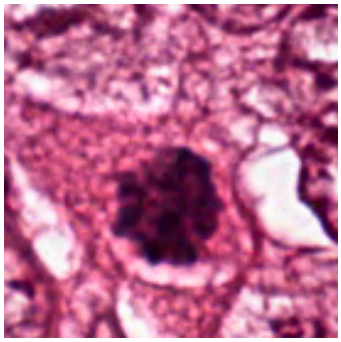

(b) CLAHE

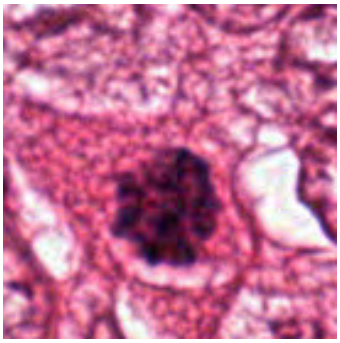

(c) Local Laplacian filtering

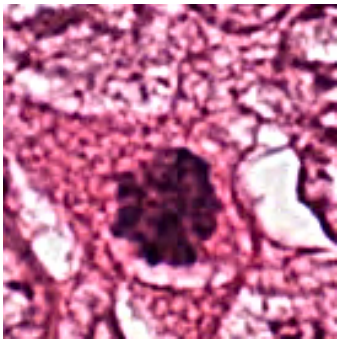

(d) Unsharp masking

Figure 5.7: A mitosis before and after applying CLAHE, local Laplacian filtering and unsharp masking.

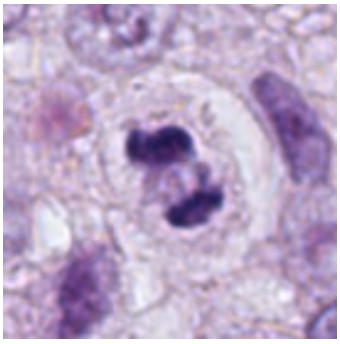

(a) Original

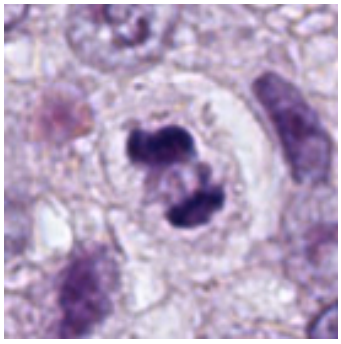

(b) CLAHE

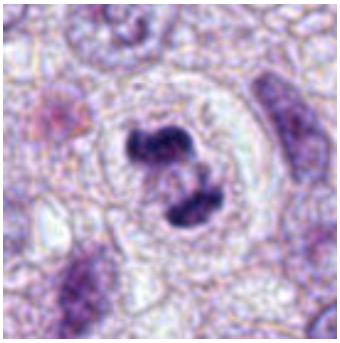

(c) Local Laplacian filtering

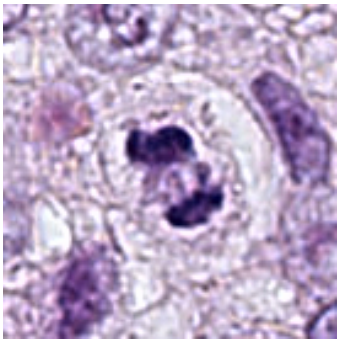

(d) Unsharp masking

Figure 5.8: A mitosis before and after applying CLAHE, local Laplacian filtering and unsharp masking.

5.2.5 K-means

The ad-hoc k-means solution where CLAHE was applied to the blue/purple cluster placed on a black background did in general improve the contrast of both mitoses and the nuclear details. The disadvantage was the boundary artefacts occurring at the edges between the blue cluster and the others when they were stitched together. An example of the output from the k-means and CLAHE approach is depicted in Figure 5.9(b). A key observation is that nuclei tend to belong to several clusters (gray and black) as illustrated in Figure 5.9(c). The content of the main nuclear cluster is shown in Figure 5.9(d).

Since k-means is an iterative procedure convergence to the global optimum is not guaranteed. But in the tested cases the algorithm appeared to converge to the same solution.

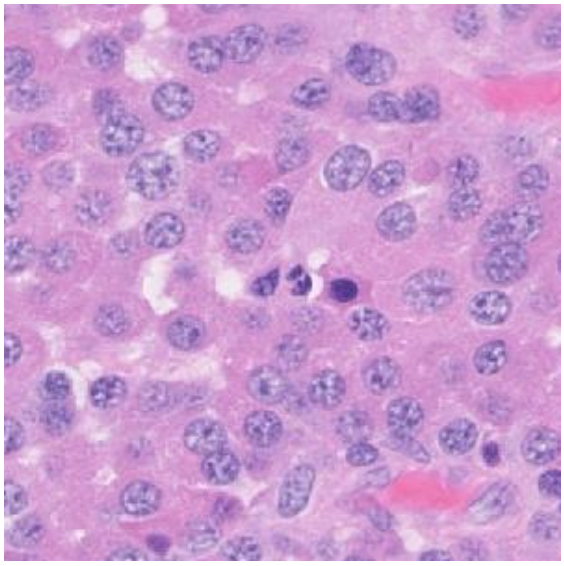

(a) Example image with mitosis in anaphase that was input to the k-means procedure.

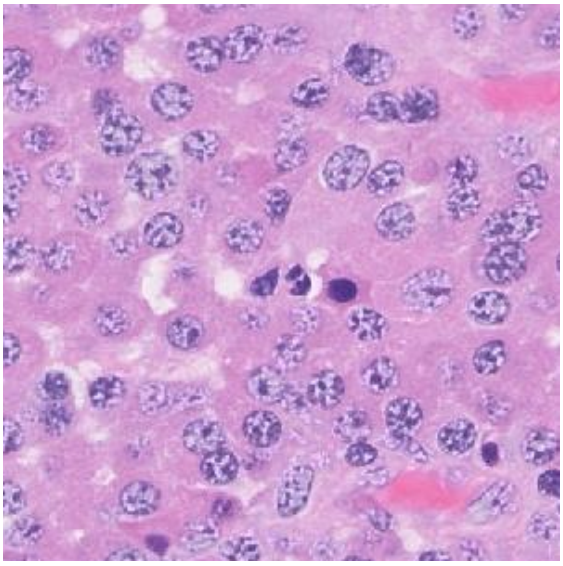

(b) The enhanced image after applying CLAHE to the blue cluster image.

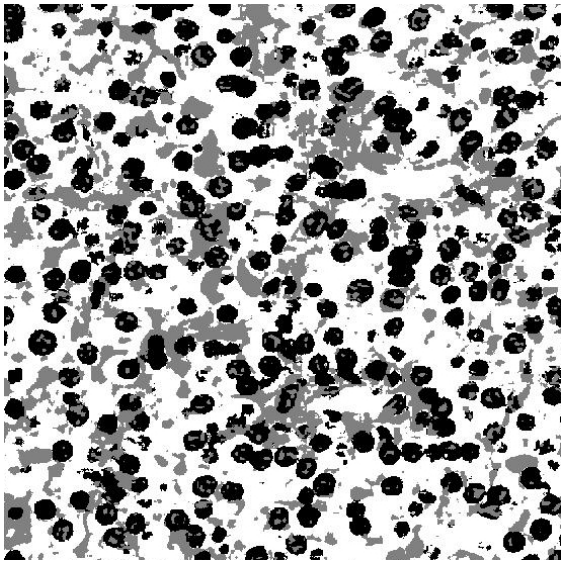

(c) Image depicting the three clusters as white, gray and black pixels.

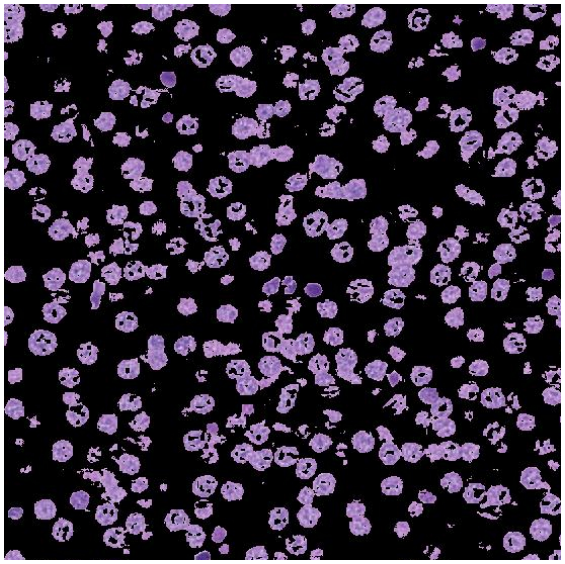

(d) The content of the blue cluster represented as an RGB image. The black pixels were not part of the cluster.

Figure 5.9: K-means and CLAHE applied to example image. The images on top are cropped to more clearly depict the mitosis.

5.3 Validation with Pathologist

The earlier reported observations agreed to a certain amount with the pathologist validation. The most unexpected outcome was the positive attitude towards images processed with CLAHE.

The scores of enhanced images compared to the unprocessed ones, are given in Table 5.3 and 5.4. The former covers the details of mitotic figures and the latter general image quality. Since processed images in the test occurred on both sides in the pairwise comparisons, a *much better* answer sometimes referred to the processed image being better and vice versa. For presentational purposes the answers from pairs where the unprocessed image was to the right were negated, meaning that a *slightly worse* answer was converted into a *slightly better* score in the tables.

Table 5.3: Mitotic figure display quality. Frequency of each score for CLAHE, Local Laplacian Filters (LLF) and Unsharp Masking (USM)

Alg. \ Score	*much worse*	*slightly worse*	*same*	*slightly better*	*much better*
CLAHE	0	2	4	5	1
LLF	0	1	6	5	0
USM	0	0	3	8	1

Table 5.4: General image quality. Frequency of each grade for the different algorithms CLAHE, LLF and USM

Alg. \ Score	*much worse*	*slightly worse*	*same*	*slightly better*	*much better*
CLAHE	0	0	2	10	0
LLF	0	1	1	10	0
USM	0	1	1	10	0

The two image pairs that reappeared at the end of the test obtained the same score at both occurrences, indicating consistency of the pathologist. Only one pair of each duplicate is included in the results. A general comment shall be made that the pathologist found it a bit strange to judge the display quality of mitotic figures when some of them, such as the tripolar one, was so clear already prior to processing.

The two-sided sign tests for matched pairs did reject the null hypothesis of equal median to the alternative hypothesis of altered general image quality for all three algorithms. The tests were carried out at significance level $\alpha = 0.05$. Regarding the details of the mitotic figures the null hypothesis could only be rejected for unsharp masking. A summary of the statistical outcome is found in Table 5.5. The shift towards improvements of the images in Tables 5.3 and 5.4 let us conclude better images in the cases where H_0 is rejected.

Table 5.5: Test decisions for the different algorithms with respect to general image quality and details of candidate mitotic figures ($\alpha = 5\%$).

Algorithm	Mitosis Details	General Quality
CLAHE	H_0, $p = 0.29$	H_1, $p < 0.01$
LLF	H_0, $p = 0.22$	H_1, $p < 0.05$
USM	H_1, $p < 0.01$	H_1, $p < 0.05$

5.4 Implementation in Sectra's Pathology Viewer

The CLAHE implementation in the viewer worked well for general contrast improvements but was less successful enhancing mitotic figures. This was due to the earlier mentioned darkening effect of the algorithm. In Figure 5.10 the side-by-side view used for comparison between the original (left) and processed (right) image is seen.

The implementation ran smooth in side-by-side view using 40X magnification due to the small region displayed on the screen. If large movements in the slide navigation were made some time, roughly two to three seconds, was needed for rendering. The centre tiles are retrieved first from the server meaning that the region where the pathologist is most likely to look will be rendered first.

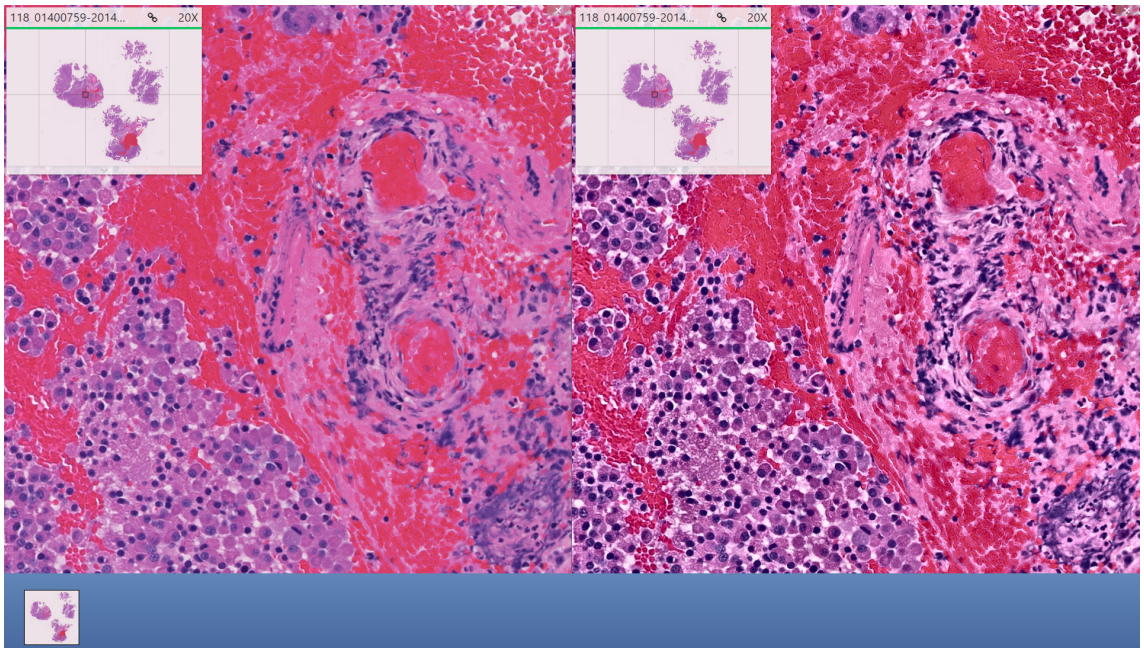

Figure 5.10: An example of the side-by-side view in the viewer

.

Chapter 6

Discussion

Several observations that can be useful in image enhancement of digital pathology images have been made. Here these findings are described, discussed and developed.

6.1 General Discussion

Is image processing to enhance mitotic figures necessary? Most mitotic figures included in mitotic counts are so easily spotted that no processing is necessary. In the consensus statement *Prognostic factors in breast cancer* it was recommended to only count definite mitotic figures [18]. When enhancement is necessary to distinguish mitoses from other entities, these mitotic figures would normally have been omitted. Thus, using image enhancement it might be necessary with a revision of the guidelines. The most important benefit of successful enhancement would be reduced examination times. In general nuclear details were easier to emphasize than mitotic figures. All algorithms could depict e.g. nucleoli inside nuclei more clearly.

Regarding suitable colour spaces for image processing of digital pathology images it is recommended to use a representation where intensity and chromaticity are separated. Since only the intensity was processed using CLAHE and unsharp masking similar results are expected from L*a*b* using Cartesian coordinates as HSV using cylindrical. L*a*b* seemed to give slightly more visually attractive results according to subjective ocular inspection, non-surprisingly since it is designed to mimic the human visual response. Another observation concerns the perceived colours. When only the intensity values were processed the colour was supposed to stay the same. However, differentiating between the luminosity and chromaticity is not easy perceptually. Decreased intensity values of a nucleus gives a perceptually of a darker purple, although the actual chromaticity is unchanged.

6.2 Image Issues

In the literature review mainly studies comparing digital pathology to examinations in light microscopes were found. Maybe more effort should have been put in the selection of the problem to approach. In the examination of mitotic figures pathologists use their experience a lot and the criteria for identification are not definite. An easier target structure would provide a clear objective for the processing.

The fact that micro-organisms are hard to see, mainly in the digital environment but also in a light microscope, is most likely difficult to address with image processing. Scanning at higher magnification, e.g. 60-80X, could probably reduce the level of difficulty as suggested by a pathologist. In the near future, coping with the increased amounts of data and computational demand that higher magnification implies should be possible.

Digital pathology images are quite unique in their character due to the sparsity in colour. As was illustrated by the histograms in Figures 5.1 and 5.2 mitoses often populate the lower range of a colour space's intensity channel. This is obvious and explains the success of pathologists quickly spotting candidate mitoses due to the pop-out from the background.

Homogeneity was found to be an important characteristic when processing the images. In general homogeneous tissue typically are restricted both in colour and intensity in a HSV or L*a*b* representation. If only cellular entities with a high affinity for one of the stains are present, the spread in a colour space will obviously be smaller than otherwise. This is only a concern for local Laplacian filters and the combinations of CLAHE and k-means/colour deconvolution where the colour channels are processed.

6.3 Algorithms

The considered algorithms are very generic. Hence, the number of possible configurations results in difficulties determining if effects are a consequence of the algorithm itself or the choice of the parameter values. A summary of the pros and cons with the different algorithms are found in Table 6.1. The computational complexity of colour deconvolution and k-means in combination with CLAHE has not been investigated.

Table 6.1: Summary of the different algorithms' strengths and weaknesses.

Algorithm	**Strengths**	**Weaknesses**
CLAHE in L*a*b* or HSV	• General • Different target histograms possible • Allows real-time implementation	• Dark output images • Mitotic figures grow
Colour Deconvolution and CLAHE	• Targets nuclear details • Different target histograms possible. • Allows real-time implementation	• Relying on stain matrices. • Artefacts • Mitotic figures grow
K-means and CLAHE	• High contrast in nuclei • Pixels outside processed cluster unchanged	• Border artefacts • Low generalization possibilities
Local Laplacian Filters	• Good contrast in mitotic figures with loose chromatin • Many tuning possibilities • Multi-scale	• Changes chromaticity • Computationally demanding
Unsharp Masking	• Good contrast in mitotic figures with loose chromatin • Fast • Intuitive parameters • Unchanged chromaticity	• Amplification of background noise

6.3.1 CLAHE

CLAHE, by construction, increased the local contrast of hematoxylin-eosin images. If a uniform target distribution is used there are two main problems. At a large scale there will after processing be structures in each tile with as low intensity values as mitoses. This affects the pop-out effect, the possibility to quickly identify candidate mitotic figures, negatively. At a smaller scale the individual mitotic figure will grow and become darker since it is likely the darkest part of the tile.

The reason that the phenomena above occur is simply that the goal of standard CLAHE is to achieve a uniform histogram. As claimed in Section 5.1 the intensity of chromatin dense mitotic figures typically have a lightness in the range 5-40. During the redistribution of pixel values in CLAHE counts are added in the lowest part of the allowed range. As an example, assume that the lowest lightness found in the original image is twenty. CLAHE will probably map these pixels to new values just above zero to increase the contrast and maximize the dynamic range. The problem is that with purple hues it is very difficult to distinguish details when the intensity is low.

Nuclei are one of the cellular entities that tend to get dark after CLAHE, e.g. in Figure 5.3 the nuclei are easier to identify in the processed image. This effect is good for emphasizing the localization of the nucleus and the chromatin pattern. Nucleoli may be hard to see in too dark nuclei.

The attempt to preserve the brightness by scaling with the ratio between the old and enhanced means suffered from problems with saturation. To improve this approach the procedure could probably use the local mean instead, computed in a sliding window.

When processing in L*a*b* and HSV was compared using paired t-tests of the RGB mean values, the null hypothesis of equal was rejected for the red and blue channels. This is intuitive since the hematoxylin-eosin images are rich in red and blue colouring. If a difference will occur somewhere it should be on those channels. High values on the green channel are mainly present in white background regions.

With gained knowledge, CLAHE using histogram specification seem better suited for enhancing mitotic figures than the ordinary algorithm with uniform target distribution. With a Rayleigh target distribution good results could be obtained on a case to case basis. In Figure 5.4 the enhanced mitotic figure to the right is seen in more detail as well as the nuclei in surrounding cells. On the other hand, the pop-out effect of the mitotic figure is decreased. There are certainly better target distributions than the Rayleigh distribution. Consider e.g. a distribution consisting of two bell-shapes, one containing the intensities dominated by mitoses and one containing the background. Investigation thereof has not been performed.

6.3.2 Colour Deconvolution

The novel combination of colour deconvolution and CLAHE worked, as long as the stain matrix was matched to the image. It is clear in Figure 5.5 that mainly nuclear structures are affected. If the separation is poor epithelium, muscle, blood cells and other structures with high affinity for eosin will impact the hematoxylin channel. Sometimes it is hard to decide whether the darkening of the eosin-stained parts after processing should be explained by unsatisfying deconvolution or that the tissue actually has an affinity for both dyes.

As mentioned in Section 2.2.3 basophilic cytoplasm usually surround mitotic figures. This could partially or fully explain the growth of mitotic figures when CLAHE is

applied to either intensity values in L*a*b* or HSV, or to the hematoxylin channel after colour deconvolution. The intuition is that the cytoplasm encapsulating the candidate mitotic figure is darker than normal cytoplasm, thus ending up even darker.

When regions of interest were selected to compute image specific stain matrices the algorithm did not work well at all times. Here the usage of snapshots was a restriction. The full digitized slides should have been used to allow identification of regions with mainly a single stain. In the snapshots from the MITOS dataset, Figures A.1(a), A.1(b), A.1(c), A.1(d) and A.1(e), it is certainly hard to select regions stained with mainly hematoxylin. Using the approach at a pathology department should be easier because stain vectors could be measured from slides stained with a single dye.

6.3.3 Local Laplacian Filtering

Since digital pathology images are stored in the pyramidal format as mentioned in Section 2.1.3 it was reasonable to consider multi-resolution techniques such as pyramidal processing. Because pathologists use the fuzziness of mitotic figures for identification, edge-aware local Laplacian filtering was considered interesting.

At first glance it might seem strange to consider a technique not affecting the edges of mitotic figures to enhance display of the latter. The reason was two-fold. In phases of mitosis when the chromatin is less dense local Laplacian filtering did improve the contrast within the mitotic figure as seen in Figures 5.7(c) and 5.8(c) respectively. Moreover, the contrast change surrounding the mitotic figure could eventually make the mitosis more easy to distinguish. As one of the interviewed pathologists described, cellular membrane of a candidate mitotic figure is informative. Here local Laplacian filters works well since such edges tend to be so vague that they are considered as details.

No optimization of the number of levels in the pyramids was done. Using a top level of 2 x 2 coefficients is most likely superfluous for enhancing structures of the size of mitoses. To compute the image pyramids snapshots of whole-slide images were used. If the levels of a whole-slide image in pyramidal format shall be used instead, it might be necessary with additional blurring.

There are reasons for not processing the full images with local Laplacian filters; both the risk of background distortion and the computational demands are reduced. If mitotic figures could be separated from the background, using segmentation or a user-provided mask, only the coefficients corresponding to mitoses in the output Laplacian pyramids would have to be calculated. In that setting only the mitotic figures have to be considered when designing the remapping function.

6.3.4 Unsharp Masking

Unsharp masking was the only sharpening technique considered due to its universality. It is the simplest of the investigated algorithms and also obtained the best results in the validation with the pathologist. Moreover it would be easy to implement intuitively in a viewer with a slider for adjusting k and maybe also the radius of the Gaussian filter.

Applying a small amount of sharpening to an unsharpened image will probably always improve the perceived quality. At least as long the background not becomes noisy, as in Figures 5.7(d) and 5.8(d). However, mitoses are seldom examined this closely, why the effect becomes a bit exaggerated.

6.3.5 K-means and CLAHE

The combination of k-means and CLAHE increased the contrast of nuclear structures. Compare the chromatin pattern in the nuclei in Figure 5.9(a) to those in Figure 5.9(b). However boundary artefacts between the processed cluster pixels and the pixels of other clusters were visible in other images. To obtain a robust method clever stitching is necessary at the cluster boundaries.

Another drawback with this method is the lack of mathematical rigour. Placing the blue cluster on a black background, in order of letting the black pixels be remapped to the darkest intensities, does the job. The result might be unpredictable.

In the hematoxylin-eosin stained images it was easy to find the cluster containing most of the nuclei using the information of the L*a*b*colour channels. In HSV it would probably have been even easier, using only the hue values.

6.4 Validation

Clearly image processing has a role to play within digital pathology. The question to be answered is rather which algorithms to use depending on the clinical application.

6.4.1 Pathologist Validation

Despite the small number of test images, significant improvements of both mitotic figures and general image quality were obtained using unsharp masking. For local Laplacian filters and CLAHE only improved general image quality could be verified.

It should be pointed out that there are several shortcomings of the test session. Only one pathologist participated and pathology is a medical discipline relying on personal experience and subjective opinions. Moreover, only twelve image pairs

were used and the algorithms had identical parameter values for all images. The two image pairs appearing twice getting the same score both times was a good sign of consistency.

The way images were displayed during the validation session is very different from how a pathologist normally work. Only snapshots were provided at a single zoom-level. In addition, the participating pathologist experienced it a bit difficult to relate the display quality of obvious mitotic figures to one another. Comments regarding a visual difference but that both the processed and unprocessed mitotic figure were so certain that the processing was unnecessary was mentioned. It would have been interesting to instead use really difficult cases where the enhancement could be the difference between being able to tell if it is a mitotic figure or not.

It is likely that there is some bias in this sort of assessment. The scale was picked to be symmetric and the images switched sides to reduce such problems. The full range of the scale was not used. In total only two *much worse/better* scores were given. With this low amount of samples, individual choices have visible effects in the final results.

The sign test only utilizes information concerning which image is better. Therefore, negating scores to produce Tables 5.3 and 5.4 should be a valid approach. This results in a weaker test but statistical conclusions made from it are more certain than if e.g. a Wilcoxon signed-rank test had been used. The latter also incorporates information regarding how much better an image is scored to be. The main concern with the sign-tests are the high number of neglected ties. First of all it violates the assumption of a binomial distribution of T. In addition, leaving out information is often suboptimal.

In a better validation session several pathologists should count mitotic figures in both enhanced and unprocessed images, preferably in their whole-slide viewer of choice. The time for investigating ten high-power-fields and the accuracy of the count could thereafter be used to determine whether the enhanced or original images are preferred. Such an approach would require much of both programming and time from clinicians, making it it unrealisable in this study.

6.4.2 Objective Validation

The image quality assessment index SSEQ appeared to be unreliable for use in digital pathology. Since the algorithm is trained on a dataset of ordinary photographs, this was not unexpected. The fact that SSEQ indicated better image quality of images processed in L*a*b* compared to HSV in Table 5.2 might be nothing but a coincidence. However, some correlation between the index and human observers is expected since distortions such as blur appear similar in different types of images. Examples such as the image ruined by adaptive histogram equalization in Figure 4.3 let us conclude that the index cannot be relied on in this particular application.

Training a no-reference image quality assessment index such as SSEQ on a database consisting of digital pathology images would be interesting. Then the main distor-

tions present in pathology images could be considered during training. The whole-slide images are often subject to lossy compression which could be one thing to measure. Moreover the focus should be considered.

6.5 Implementation in Viewer

The CLAHE implementation in Sectra's viewer was not tested in a clinical setting. The area of the nine tiles that where used to extract a single tile was purely ad-hoc. It may be sufficient to use less of the neighbouring tiles which would result in a faster algorithm.

Due to the variety of tasks that a pathologist may perform it should be made possible to manually change the clip limit. Probably it would be sufficient with three different settings such as *low*, *medium* and *high*, referring to the contrast changes. A continuous slider would likely incorporate some lag due to the need for real-time processing. In the used setup the server was a weak virtual machine. If a physical server had been used huge speedup should be expected. Client-side processing could be an alternative since CLAHE is highly parallelizable.

6.6 Limitations

Only hematoxylin-eosin images have been considered. Because CLAHE and unsharp masking were applied to pixel intensities, their behaviour can be expected to be similar if other stains are used.

During the interviews it became obvious that pathology, similar to many medical disciplines, rely on experience. Hence opinions and ideas from more pathologists would have been desirable.

The practice of pathology is to a large extent a science of experience. Thus it can be hard to make unbiased tests of new image processing regimes. Presumably, a quite drastic change towards the better is required to receive good feedback.

6.7 Ethics

In medical image enhancement a key concern is the relation between images and the reality that they are describing. It is considered important to always let pathologists be aware of any image processing applied to the images they are examining. In the worst case scenario, artefacts from image enhancement may result in incorrect diagnoses. As mentioned in Section 2.2.2 dark nuclei may be a sign of anaplasia. Thus applying contrast enhancement without awareness of the pathologist may be troublesome since many structures tend to end up darker.

Digital pathology in general is discussed from an ethical viewpoint in [2]. It is argued that with digital reviews, developing countries can take part of the expertise from pathologists abroad. Moreover, enhancement of mitotic display could improve the ergonomics of pathologists. If they confidently could count mitotic figures on a computer screen instead of in a microscope, neck problems would diminish.

For the environment, colour deconvolution offer possibilities to reduce the amount of staining since the experienced stain quantity can be increased artificially. Anyhow the use of hematoxylin and eosin is not known to be a major environmental issue.

Chapter 7

Future Work

Today digital pathology is always compared to conventional pathology using a microscope. As the digital technology conquers the market several things will change. Most pathologists today learnt the profession using a light microscope and literature written accordingly. Moreover, stains such as hematoxylin and eosin have been used for a very long time, despite that the contrast between purple and pink is bad. Obviously, there are colours that offer better possibilities for discrimination. It would be interesting to observe the outcome of stains where the hues differ by 180 degrees in a HSV representation. Such an approach was taken by Landini and Perryer to reduce the problems that colour blind observers experience with hematoxylin-eosin images [53]. If pathology will be a digital discipline in the future, new stains applied either digitally or physically will likely occur.

Technological progress can hopefully diminish the focus problems of whole-slide images. As connection speeds, computational power and storage capabilities increase, specimens can be scanned at higher magnification and in multiple focus planes. With higher baseline magnification the level of detail of nuclei and mitotic figures increases. Then image enhancement might be superfluous. Several focus planes increases the likelihood of good focus in at least one of these. Moreover it gives a feeling for the three-dimensional structure of objects, useful in assessment of mitotic figures. The only disadvantage mentioned with multiple focus layers mentioned by the third pathologist was large storage requirements, which will be a smaller problem as technology progress.

If the use of image processing increases in clinics, colour deconvolution could play a key role. It can be used for stain quantification, colour normalization and as shown earlier to enhance the contrast of certain cellular entities. Much can be gained from standardizing stain matrices for different combinations of scanners and stains. Colour deconvolution could then be used with higher confidence, obtaining more accurate separation of the stains. It would be helpful to be able to estimate how well a stain matrix fits an image. To some extent this can be done using the residual channel, but more accurate methods could likely be developed. The novel combination of colour deconvolution and CLAHE yet has to be validated. However, it will make mitotic figures with basophilia in the surrounding cytoplasm

darker.

It could be argued that enhanced display of mitoses is unnecessary since in a few years from now the machine learning algorithms for mitosis counting probably outperform pathologists. It may be true that the performance of machines will improve dramatically, but as long as the person that is legally responsible for the diagnosis is the pathologist, an introduction to the clinic is unlikely. Especially deep-learning algorithms, probably the hardest ones to understand, have showed considerable success in mitosis detection. A realistic scenario might be that in a few years algorithms will localize the most active parts of tumours and thereafter suggest candidate mitoses in that region. Finally a pathologist can verify the results. That last step would benefit from increased display quality.

For image enhancement of digital pathology images there are two main roads. The first is to implement general image processing tools in the viewers and thereafter let pathologists do adjustments on a case by case basis. Alternatively, standardized image enhancement protocols with task-specific image processing can be developed for frequent examinations.

Mitotic figures are present in many different tissue types such as skin and breast. Since breast tissue is so homogeneous and a main application of mitotic counts it could be an idea to develop algorithms for this tissue solely. Local Laplacian filters appeared to increase the details of mitotic figures in these images without altering the surrounding tissue much.

Concerning the CLAHE implementation in Sectra's viewer there are a lot to improve. A parallel client-side implementation would probably increase the performance. It might be possible to avoid interpolation and instead compute a mapping for every single pixel using a small window. Allowing other target distributions than uniform would increase the number of possible applications. In order of not destroying the pop-out effect it is worth considering not to change the global contrast but instead use some sort of magnifier. This could be used to look at individual mitosis-candidates. In such a tool more dramatic image processing could be used. It would also be obvious for the pathologist how the candidate mitotic figure looked with and without the magnifier.

These are only a few thoughts of how the development of digital pathology and examinations of mitotic figures can progress. The direction will be determined by adoption both in medical education and clinics and legal legislations.

Chapter 8

Conclusions

Unsharp masking significantly improved both display quality of mitotic figures and general image quality. Local Laplacian filters and CLAHE only improved image quality in the test set. Applying CLAHE to hematoxylin-eosin images tend to make mitotic figures both darker and larger. This holds both in L*a*b* and HSV. A low normalized clip limit is recommended to limit contrast changes.

A novel method for contrast adjustment of nuclear details was proposed, consisting of a combination of colour deconvolution and CLAHE. The method improves the contrast in nuclear structures whilst other regions are less affected. The clinical usefulness yet has to be validated.

CLAHE was integrated in Sectra's viewer software for digital pathology images. The algorithm's complexity allows real time rendering by a low performance server.

Appendix

Images with Mitotic Figures

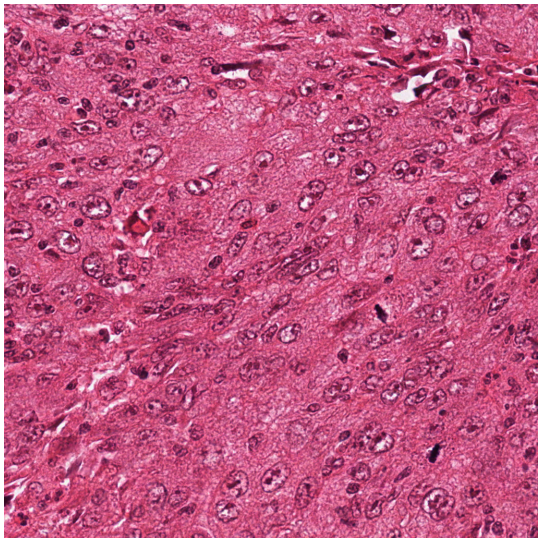

(a) Breast, MITOS, Aperio scanner

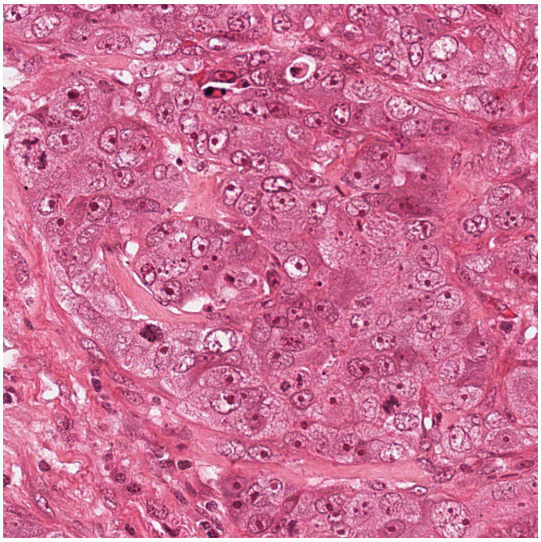

(b) Breast, MITOS, Aperio scanner

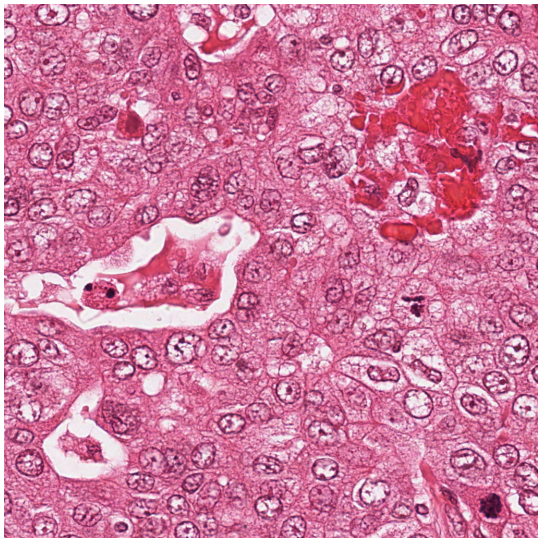

(c) Breast, MITOS, Aperio scanner

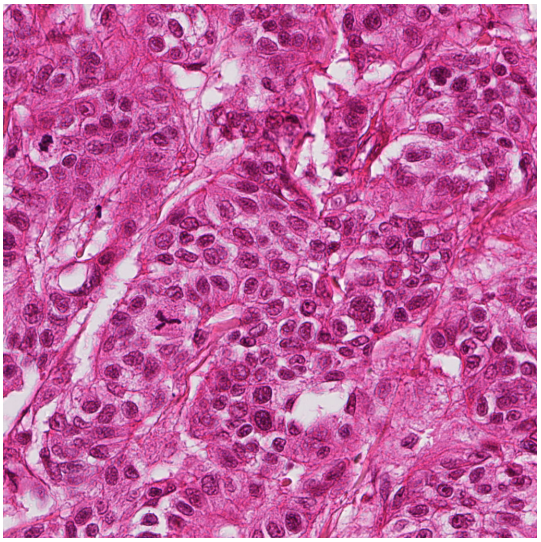

(d) Breast, MITOS, Hamamatsu scanner

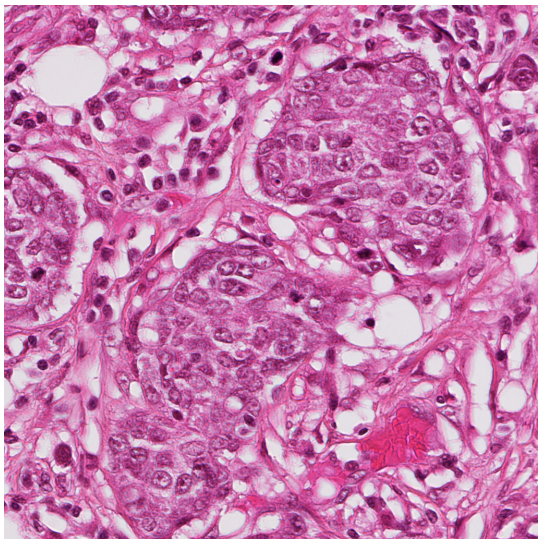

(e) Breast, MITOS, Hamamatsu scanner

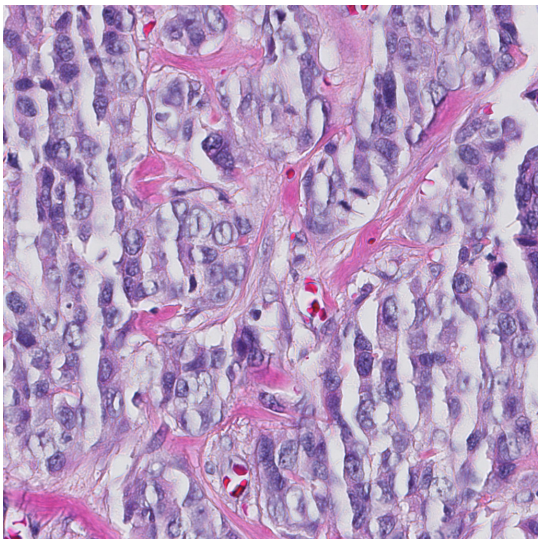

(f) Tissue with fixation problems, Hamamatsu scanner

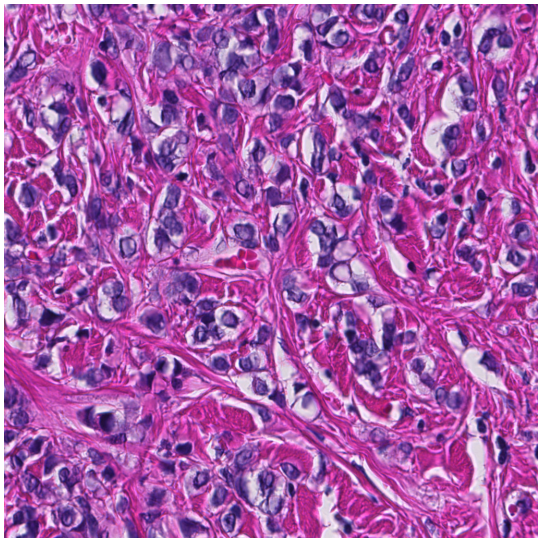

(g) High amount of stain, Hamamatsu scanner

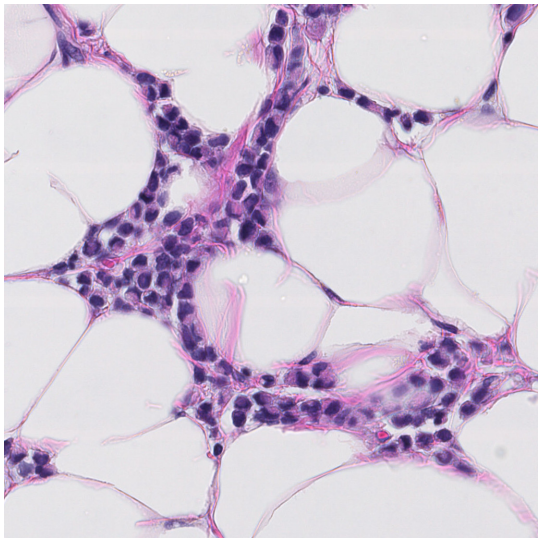

(h) Breast tissue and fat, Hamamatsu scanner

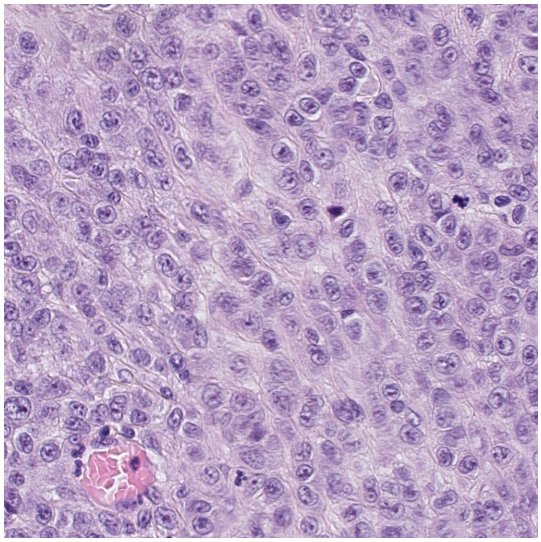

(i) High affinity for hematoxylin, Hamamatsu scanner

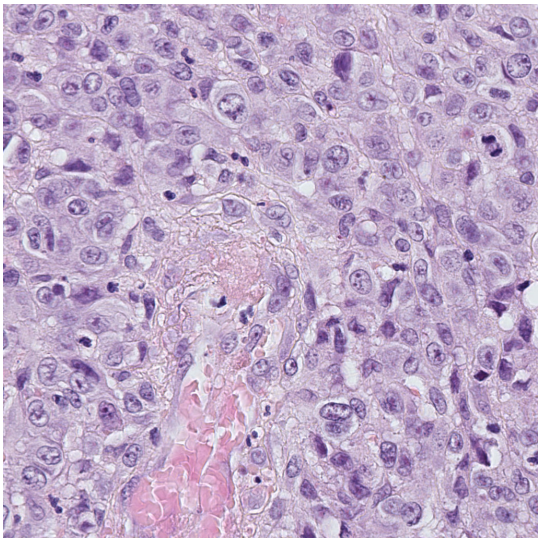

(j) High affinity for hematoxylin, Hamamatsu scanner

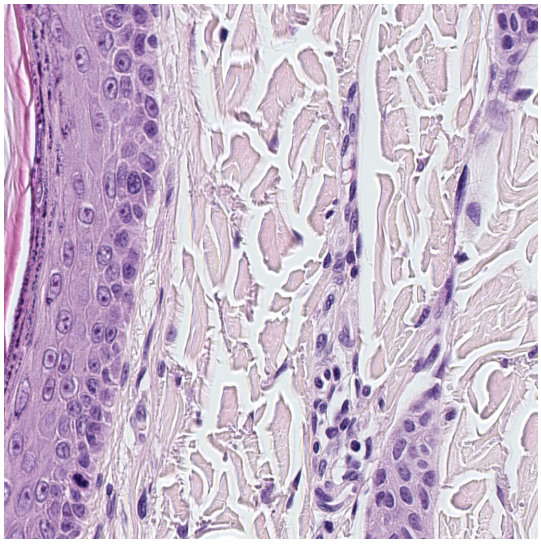

(k) Skin, Hamamatsu scanner

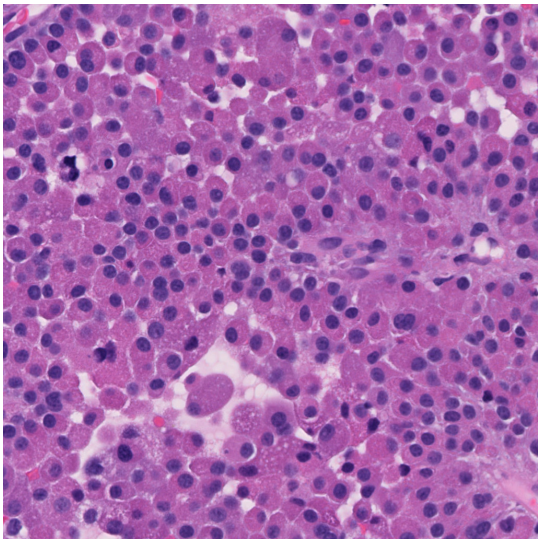

(l) High affinity for hematoxylin, Hamamatsu scanner

Figure A.1: Image dataset with mitotic figures. Images (a)-(e) are from the MITOS datset. The others have been taken from different whole-slide images whereafter their clinical relevance was confirmed by a pathologist.

Bibliography

[1] V. Kumar, A. K. Abbas, and J. C. Aster, *Robbins Basic Pathology, 9th ed.* Philadelphia: Elsevier, 2013.

[2] K. J. Kaplan, L. K. F. Rao, and T. C. Allen, *Digital pathology : historical perspectives, current concepts & future applications.* Cham, Switzerland : Springer, 2016.

[3] World Health Organization, *World Cancer Report 2014.* Geneva: WHO Press, 2014.

[4] A. W. Rogers, *Cells and Tissues: An Introduction to Histology and Cell Biology.* London: Academic Press Inc, 1982.

[5] "Tissue processing 14." `https://flic.kr/p/qkZxk`. by Ed Uthman, CC BY-SA 2.0, Accessed: 01-Jun-2016.

[6] "Optical microscope nikon alphaphot." `https://commons.wikimedia.org/wiki/File:Optical_microscope_nikon_alphaphot_%2B.jpg`. by Moisey, CC BY-SA-3.0, Accessed: 06-Jun-2016.

[7] "Digital Pathology Association." `https://digitalpathologyassociation.org/about-digital-pathology`. Accessed: 07-Mar-2016.

[8] Y. Sucaet and W. Waelput, *Digital Pathology.* New York: Springer, 2014.

[9] K. J. Arrow, L. Hurwicz, and H. Uzawa, "Validation of digital pathology imaging for primary histopathological diagnosis," *Histopathology*, vol. 68, no. 7, pp. 1063 – 1072, 2015.

[10] B. Alberts *et al.*, *Essential Cell Biology, 3rd edition.* New York: Garland Science, 2010.

[11] B. Alberts *et al.*, *Essential Cell Biology, 4th edition.* New York: Garland Science, 2014.

[12] J. Baak, "Mitosis counting in tumors," *Human Pathology*, vol. 21, no. 7, pp. 683 – 685, 1990.

[13] P. Dey, "Chromatin pattern alteration in malignant cells: an enigma.," *Diagnostic Cytopathology*, vol. 32, no. 1, pp. 25 – 30, 2005.

[14] J. Segen, *The Dictionary of Modern Medicine*. New Jersey: Parthenon Publishing Group, 1992.

[15] C. W. Elston and I. O. Ellis, "Pathological prognostic factors in breast cancer. 1. the value of histological grade in breast cancer: experience form a large study with long-term follow-up.," *Histopathology*, vol. 19, pp. 403–410, 1991.

[16] J. Jobsen *et al.*, "The prognostic relevance of the mitotic activity index in axillary lymph node-negative breast cancer.," *Breast Cancer Res Treat*, vol. 149, pp. 343–351, 2015.

[17] P. Donizy, M. Kaczorowski, M. Leskiewicz, M. Zietek, M. Pieniazek, C. Kozyra, A. Halon, and R. Matkowski, "Mitotic rate is a more reliable unfavorable prognosticator than ulceration for early cutaneous melanoma: a 5-year survival analysis.," *Oncology Reports*, vol. 32, no. 6, pp. 2735 – 2743, 2014.

[18] P. L. Fitzgibbons *et al.*, "Prognostic factors in breast cancer," *Arch Pathol Lab Med*, vol. 124, pp. 966–978, 1999.

[19] W. Burger and M. J. Burge, *Digital Image Processing*. New York: Springer, 2008.

[20] C. G. Gonzalez and E. R. Woods, *Digital Image Processing, 2nd version*. New Jersey: Prentice Hall, 2002.

[21] S. M. Pizer *et al.*, "Adaptive histogram equalization and its variations," *Computer Vision, Graphics, and Image Processing*, vol. 39, pp. 355–368, 1987.

[22] K. Zuiderveld, "Contrast limited adaptive histogram equalization," *Graphic Gems . Academic Press Professional*, vol. 4, pp. 474–485, 1994.

[23] MATLAB Image Processing Toolbox, *version 8.6 (R2015b)*. Natick, Massachusetts: The MathWorks Inc., 2015.

[24] A. C. Ruifrok and D. A. Johnston, "Quantification of histochemical staining by color deconvolution," *Anal Quant Cytol Histol*, vol. 23, pp. 291–299, 2001.

[25] M. Macenko *et al.*, "A method for normalizing histology slides for quantitative analysis," *IEEE International Symposium on Biomedical Imaging: From Nano to Macro*, pp. 1107–1110, 2009.

[26] C. M. Bishop, *Pattern Recognition and Machine Learning*. New York: Springer, 2006.

[27] K. J. Arrow, L. Hurwicz, and H. Uzawa, "Local laplacian filters: Edge-aware image processing with a laplacian pyramid," *Communications of the ACM*, vol. 58-3, pp. 81–91, 2015.

[28] "Image pyramid." `https://upload.wikimedia.org/wikipedia/commons/4/43/Image_pyramid.svg`. by Cmglee, CC BY-SA 3.0, Accessed: 06-Jun-2016.

[29] P. Burt and E. Adelson, "The Laplacian pyramid as a compact image code.," *IEEE Transactions on Communications*, vol. 31, no. 4, p. 532, 1983.

[30] M. Aubry, S. Paris, S. W. Hasinoff, J. Kautz, and F. Durand, "Fast local laplacian filters: Theory and applications," *ACM Trans. Graph.*, vol. 33, pp. 167:1–167:14, Sept. 2014.

[31] Z. Wang, A. C. Bovik, H. R. Sheikh, and E. P. Simoncelli, "Image quality assessment: From error visibility to structural similarity," *IEEE Transactions on Image Processing*, vol. 13:4, p. 600–612, 2004.

[32] L. Liu *et al.*, "No-reference image quality assessment based on spatial and spectral entropies," *Signal Processing: Image Communication*, vol. 29, pp. 856–863, 2014.

[33] S. Al-Janabi *et al.*, "Whole slide images for primary diagnostics of gastrointestinal tract pathology: A feasibility study," *Hum Pathol*, vol. 43, pp. 702–7, 2012.

[34] S. Al-Janabi *et al.*, "Digital slide images for in breast pathology: A feasibility study," *Hum Pathol*, vol. 43, pp. 2318–25, 2012.

[35] J. R. Gilbertson, "Primary histologic diagnosis using automated whole slide imaging: A validation study," *BMC Clin Pathol*, vol. 6:4, 2006.

[36] D. M. Jukic *et al.*, "Clinical examination and validation of primary diagnosis in anatomic pathology using whole slide digital images," *Arch Pathol Lab Med*, vol. 135, pp. 372–8, 2011.

[37] A. Chang, *Oncology: An Evidence-Based Approach*. New York: Springer, 2007.

[38] N. Velez, D. Jukic, and J. Ho, "Evaluation of 2 whole-slide imaging applications in dermatopathology," *Human Pathology*, vol. 39, no. 9, pp. 1341 – 1349, 2008.

[39] M. Barry, S. Sinha, M. Leader, and E. Kay, "Poor agreement in recognition of abnormal mitoses: requirement for standardized and robust definitions.," *Histopathology*, vol. 38, no. 1, pp. 68 – 72, 2001.

[40] D. Treanor, B. D. Gallas, M. A. Gavrielides, and S. M. Hewitt, "Evaluating whole slide imaging: A working group opportunity," *J Pathol Inform.*, vol. 6:4, 2015.

[41] C. Malon *et al.*, "Mitotic figure recognition: Agreement among pathologists and computerized detector.," *Analytical Cellular Pathology: Cellular Oncology*, vol. 35, no. 2, pp. 97 – 100, 2012.

[42] S. Al-Janabi, H.-J. van Slooten, M. Visser, T. van der Ploeg, P. J. van Diest, and M. Jiwa, "Evaluation of mitotic activity index in breast cancer using whole slide digital images.," *PLoS ONE*, vol. 8, no. 12, pp. 1 – 9, 2013.

[43] P. Donizy, M. Kaczorowski, M. Leskiewicz, M. Zietek, M. Pieniazek, C. Kozyra, and R. Matkowski, "Mitotic rate is a more reliable unfavorable prognosticator than ulceration for early cutaneous melanoma: A 5-year survival analysis," *Oncology Reports*, vol. 32, pp. 2735–2743, 2014.

[44] L. Roux, "MITOS dataset." `http://ludo17.free.fr/mitos_2012/dataset.html`. Accessed: 04-Mar-2016.

[45] L. Roux *et al.*, "Mitosis detection in breast cancer histological images: An ICPR 2012 contest," *J Pathol Inform*, vol. 4, no. 1, p. 8, 2013.

[46] G. Bradski *Dr. Dobb's Journal of Software Tools*, 2000.

[47] S. van der Walt, J. L. Schönberger, J. Nunez Iglesias, F. Boulogne, J. D. Warner, N. Yager, E. Gouillart, T. Yu, and the scikit-image contributors, "scikit-image: image processing in Python," *PeerJ*, vol. 2, p. 453, 2014.

[48] B. Jähne, *Digital Image Processing*. Berlin-Heidelberg: Springer-Verlag, 2005.

[49] G. Landini, "Colour Deconvolution." `http://www.mecourse.com/landinig/software/cdeconv/cdeconv.html`. Accessed: 01-Jun-2016.

[50] C. A. Schneider, W. S. Rasband, and K. W. Eliceiri, "NIH image to ImageJ: 25 years of image analysis," *Nature methods*, vol. 9(7), 2012.

[51] P. H. Kvam and B. Vidakovic, *Nonparametric Statistics with Applications to Science and Engineering*. New Jersey: John Wiley & Sons Inc, 2007.

[52] C. Huang, "Emgu CV." `http://www.emgu.com`, 2010.

[53] G. Landini and G. Perryer, "Digital enhancement of haematoxylin- and eosin-stained histological images for red–green colour-blind observers.," *Journal of Microscopy*, vol. 234, no. 3, pp. 293 – 301, 2009.